USGS
science for a changing world

Chemical Evaluation of Water and Gases Collected from Hydrothermal Systems Located in the Central Aleutian Arc, August 2015

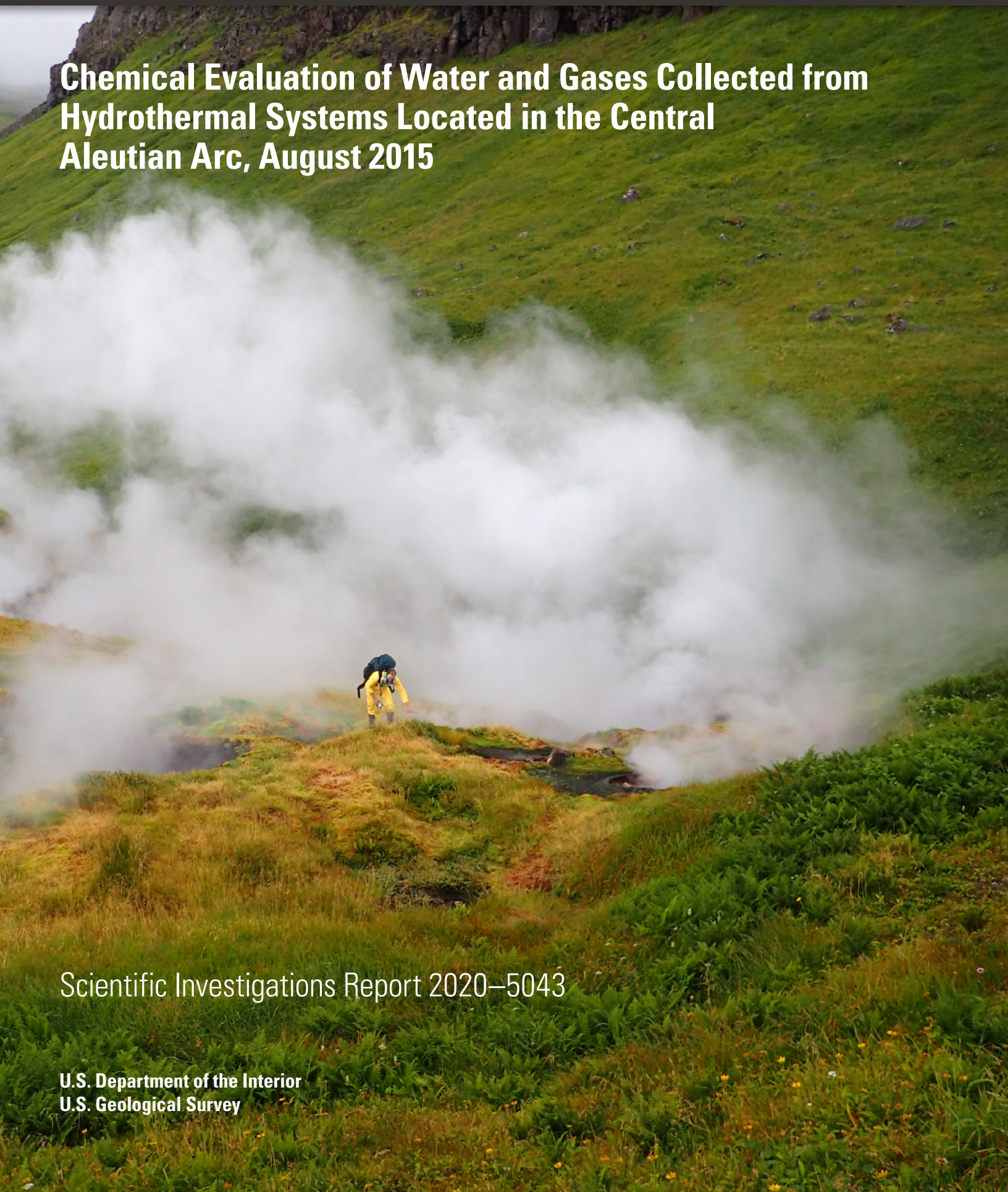

Scientific Investigations Report 2020–5043

U.S. Department of the Interior
U.S. Geological Survey

Cover. Photograph of Christoph Kern (U.S. Geological Survey) taking gas measurements between large gas plumes on Geyser Bight, Umnak Island, Alaska. Photograph by Cynthia Werner.

Back cover. Photograph of the northern interior of Fisher Caldera on Unimak Island, Alaska. The view is from mount Finch looking west-southwest. Photograph by Cynthia Werner.

Chemical Evaluation of Water and Gases Collected from Hydrothermal Systems Located in the Central Aleutian Arc, August 2015

By Cynthia Werner, Christoph Kern, and Peter Kelly

Scientific Investigations Report 2020–5043

U.S. Department of the Interior
U.S. Geological Survey

U.S. Department of the Interior
DAVID BERNHARDT, Secretary

U.S. Geological Survey
James F. Reilly II, Director

U.S. Geological Survey, Reston, Virginia: 2020

Suggested citation:
Werner, C., Kern, C., and Kelly, P. K., 2020, Chemical evaluation of water and gases collected from hydrothermal systems located in the central Aleutian arc, August 2015: U.S. Geological Survey Scientific Investigations Report 2020–5043, 35 p., https://doi.org/10.3133/sir20205043.

ISSN 2328-0328 (online)

Acknowledgments

The authors gratefully acknowledge the contributions from John Power, Deb Bergfeld, Laura Clor, Pete Stelling, and Bill Evans for their help with project planning and funding negotiations, field work preparations, analytical support, and for reviewing this report. We also gratefully acknowledge the careful review by Taryn Lopez and Phil Frederick. The authors would also like to thank JoJo Mangano for his skill in redrafting the map figures. The work would not have been possible without the field logistical support provided by Maritime Helicopters, Homer, Alaska. Funding was provided by the Alaska Volcano Observatory, the Deep Carbon Observatory, and the National Science Foundation (Grant # EAR-1456939 to Diana Roman, Erik Hauri, and Terry Plank). The science team are very grateful for the support received from Maritime Helicopter's research vessel Maritime Maid and crew, and the Bell 407 helicopter, skillfully piloted by Dan Leary.

Contents

Figures

Tables

Conversion Factors

International System of Units to U.S. customary units

Multiply	By	To obtain
	Length	
centimeter (cm)	0.3937	inch (in.)
millimeter (mm)	0.03937	inch (in.)
micrometer (μm)	0.000039	inch (in.)
meter (m)	3.281	foot (ft)
kilometer (km)	0.6214	mile (mi)
	Area	
square meter (m^2)	10.76	square foot (ft^2)
square kilometer (km^2)	0.3861	square mile (mi^2)
	Flow rate	
liter per minute (L/min)	0.26417	gallon per minute (gal/min)
	Concentration	
milligrams per liter (mg/L)	0.00000834	pound per gallon (lb/gal)

Temperature in degrees Celsius (°C) may be converted to degrees Fahrenheit (°F) as °F = (1.8 × °C) + 32.

Temperature in degrees Fahrenheit (°F) may be converted to degrees Celsius (°C) as °C = (°F – 32) / 1.8.

Datum

Vertical coordinate information is referenced to the [World GeodeticSystem 84 (WGS 84)].

Horizontal coordinate information is referenced to the [World GeodeticSystem 84 (WGS 84)].

Altitude, as used in this report, refers to distance above the vertical datum.

Supplemental Information

Concentrations of chemical constituents in water are given in either milligrams per liter (mg/L) or micrograms per liter (µg/L).

Results for measurements of stable isotopes of an element (with symbol E) in water are expressed as the relative difference in the ratio of the number of the less abundant isotope (^{i}E) to the number of the more abundant isotope of a sample with respect to a measurement standard.

Abbreviations

ASMW	Air saturated meteoric water
GeoPRISMS	Geodynamic Processes at Rifting and Subducting Margins
GMWL	Global Meteoric Water Line
GPS	Global Positioning System
ml	milliliter
NSF	National Science Foundation
ppm	parts per million
UGV	upper Glacier valley (on Makushin volcano)
µg	micrograms
µm	micrometer
USGS	U.S. Geological Survey

Chemical Symbols

Ar	Argon
B	Boron
Br	Bromide (Br^-)
Ca	Calcium
Cl	Chlorine; chloride (Cl^-)
CO_2	Carbon dioxide
HCO_3	Bicarbonate (HCO_3^-)
H_2S	Hydrogen sulfide
He	Helium
H_2	Molecular hydrogen
K	Potassium
Mg	Magnesium
N_2	Molecular nitrogen
Na	Sodium

O_2	Molecular oxygen
SiO_2	Silica
SO_2	Sulfer dioxide
SO_4	Sulfate

Notation

$\delta^{13}C$	$^{13}C/^{12}C$ in sample (C) compared to that of a standard reference
$\delta^{13}C\text{-}CO_2$	$^{13}C/^{12}C$ in sample (CO_2) compared to that of a standard reference
δD	$^{2}H/^{1}H$ in sample compared to that of standard mean ocean water
$\delta^{18}O$	$^{18}O/^{16}O$ in sample compared to that of standard mean ocean water
CO_2/S_T	ratio of carbon dioxide to total sulfur
R_C/R_A	$^{3}He/^{4}He$ corrected for atmospheric air
SO_2/S_T	ratio of sulfur dioxide to total sulfur

Chemical Evaluation of Water and Gases Collected from Hydrothermal Systems Located in the Central Aleutian Arc, August 2015

By Cynthia Werner, Christoph Kern, and Peter J. Kelly

Abstract

Five volcanic-hydrothermal systems in the central Aleutians Islands were sampled for water and gas geochemistry in 2015 to provide baseline data to help predict future volcanic unrest. Some areas had not been sampled in 20–30 years (Makushin volcano, Geyser Bight) and other areas had minimal to no prior sampling (Tana volcano and Fisher Caldera). The chemical and isotopic data of the waters show a wide variety of characteristics typical of hydrothermal settings. Stable isotopic analyses of the waters show no evidence for primary magmatic water, rather that waters have a meteoric origin that is variably influenced by boiling and evaporation processes. The carbon and helium isotopic analyses of gases suggest they contain a primary magmatic component typical of the upper mantle at most locations, and the CO_2/S ratios show that these gases have been modified by interactions with groundwater along the flow paths. Some areas demonstrate stable compositions since the last sampling (for example, Akutan hydrothermal areas), with some being remarkably steady over very long periods (for example, Geyser Bight). Other areas show modifications because of either lower amounts of upwelling from hydrothermal sources or lower amounts of magmatic influence on the surface chemistry (for example, Upper Glacial valley of Makushin, an informally named valley leading south of the volcano toward Makushin Bay to the south). Finally, this report highlights that previously unsampled regions in the Aleutian Islands, such as Tana volcano and Fisher Caldera (the latter found to have one of the highest helium isotopic signatures ever measured in the Aleutian Islands), show evidence of ongoing subsurface magmatism that warrants continued investigation in terms of volcanic hazard.

Introduction

This report summarizes the geochemistry of gases and waters collected in August 2015 from five volcanic hydrothermal systems as part of the mission to the central Aleutian Islands jointly funded by the Alaska Volcano Observatory, the National Science Foundation (NSF) Geodynamic Processes at Rifting and Subducting Margins (GeoPRISMS) Program, and the Deep Carbon Observatory. The data described herein were collected from fumaroles and hot springs at Makushin, Akutan, Tana, and Fisher volcanoes and the Geyser Bight thermal area. Sample collection was completed by Cynthia Werner and Christoph Kern of the Cascades Volcano Observatory, Vancouver WA, and analyses were performed or organized by Deborah Bergfeld of the U.S. Geological Survey in Menlo Park (methods are described in detail herein). Discussion of the hydrothermal regions is organized by threat level, with Makushin and Akutan Volcanoes representing some the highest threat volcanoes in Alaska (Ewert and others, 2005, 2018), and a map of the areas can be viewed in figure 1.

Methods

Water Sampling

Sample sites were determined based on features sampled in past studies (when available) and located using a handheld Global Positioning System (GPS) device. Whenever possible, spring samples were collected at the location where water issued from the ground, but large pools were sampled from the edge (table 1, available for download at https://doi.org/10.3133/sir20205043). The standard sampling suite included two 60-milliliter (ml) samples of filtered [0.45 micron (µm)] water in plastic bottles for bulk chemistry (including major ions and trace metals), one 15-ml sample of raw water for stable isotope (δD, $\delta^{18}O$) analysis, and two 60-ml glass bottles of raw water for alkalinity (fig. 2). Samples for cation analysis were acidified in the field to pH <2, using ultrapure nitric acid. All sample bottles, syringes, and containers were rinsed three times prior to being filled with the appropriate water (that is, bottles for the filtered samples were rinsed with filtered water). Temperature was measured in the field using a digital meter and field pH was measured using pH paper. Alkalinity titrations were performed in the lab and at that time pH was determined using a digital meter.

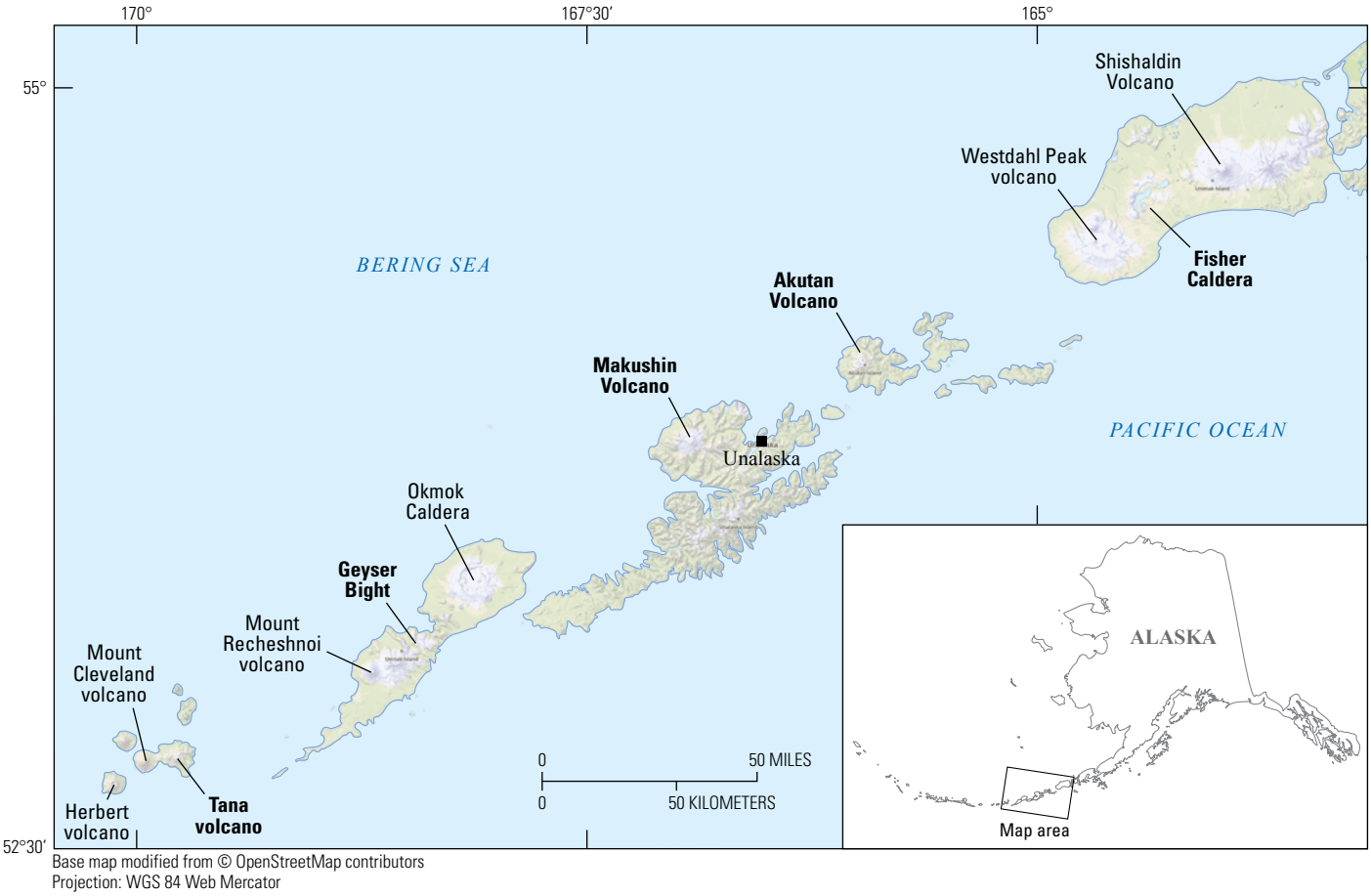

Figure 1. Map showing the central Aleutian Islands and general sample locations (in bold) from this study.

Figure 2. Photograph of water sampling at Tana volcano's north flank on Chuginadak Island. When needed, samples were collected using a beaker to allow the sediment to settle prior to filtering. U.S. Geological Survey photograph by Cynthia Werner.

Gas Sampling

Gas samples for chemistry were collected in two types of glass bottles, and gas for helium isotope analyses was collected into copper tubing. At springs that emitted gas bubbles, we used an evacuated Pyrex tube attached to a funnel (fig. 3; table 2, available for download at https://doi.org/10.3133/sir20205043). A small piece of tubing attached to a syringe was inserted into the inlet of the gas bottle to evacuate any air prior to sampling. At fumaroles, we used t-handle evacuated Pyrex sample bottles attached to a titanium tube that was inserted into the orifice of the fumarole. Gas was allowed to flow through the arms of the sample tube for a sufficient time to purge atmospheric gases. Flexible vent tubing on the downstream arm of the bottle was clamped shut and the sample tube was opened to collect the gas after the system was purged. Ice-water was used to cool the outside of evacuated tubes to aid in condensing the steam component of the gas sample. During this process the stopcock was opened to allow a vigorous flow of gas into the evacuated tube and then closed for cooling before opening the stopcock again. When the flow slowed, the sampling was stopped so that no condensed steam was lost from the sampling tube. Condensed steam was also collected from fumaroles into 15-ml glass bottles for stable isotope (δD, $\delta^{18}O$) analyses.

Figure 3. Photograph of gas sample collection at a spring on Tana volcano on the eastern side of Chuginadak Island. U.S. Geological Survey photograph by Cynthia Werner.

Chemical Analyses

Chemical analyses of the water and gas samples were performed at the U.S. Geological Survey (USGS) in Menlo Park, California following the methods of Bergfeld and others (2011), and plots were created based on Powel and Cumming (2010). Waters were analyzed for anion concentrations by ion chromatography and for cations by argon (Ar) plasma optical-emission spectrometry. Gases were analyzed using gas chromatographs equipped with thermal-conductivity, flame-ionization and pulsed discharge ionization detectors. Stable isotope analyses (δD, $\delta^{18}O$) of waters and steam condensates, and $\delta^{13}C$ on CO_2 were performed by mass spectrometry at the USGS Stable Isotope Laboratory in Reston, Virginia (table 3). Noble-gas ratios were determined by mass spectrometry at the USGS Noble Gas Laboratory in Denver, Colo. Helium-3 to helium-4 ($^3He/^4He$) ratios are corrected for minor amounts of air and are reported as R_C/R_A values.

Additional Measurements on Site—MultiGAS

In addition to the measurements described above, a USGS Multicomponent Gas Analyzer System (MultiGAS) instrument (fig. 4) was run at sites where gases were discharging from the surface. Typically, the unit was set 3–10 meter (m) downwind of a fumarole or area of vigorously steaming ground. In situ gas compositions (H_2O, CO_2, SO_2, H_2S) were measured and ratios of CO_2/H_2S are reported here (SO_2 was not detected at any of the sampled sites). The instrument included an integrated GPS receiver (Garmin GPS 18×LVC), a non-dispersive infrared CO_2 and H_2O analyzer [LI-COR, Inc. LI-840A, 0–5000 parts

Table 3. Additional stable isotope data for waters collected in the central Aleutian Islands August 11–20, 2015.

[δD and $\delta^{18}O$ are measured in per mil (‰).]

Area	Sample name	Location notes	Date	δD	$\delta^{18}O$
Background waters					
Geyser Bight	GB-05A	Stream near fumarole area		−65.15	−8.46
Geyser Bight	GB-BK			−65.25	−9.25
Makushin	MK-04	Glacial runoff		−82.29	−11.58
Fumarole Condensates					
Akutan	AK-06F	Flank fumarole	08/21/15	−64.88	−9.51
Fisher	FI-01F	Mount Finch	08/19/15	−102.96	−16.08
Geyser Bight	GB-08F	Area G	08/16/15	−93.43	−13.85
Geyser Bight	GB-01F	Area F1	08/16/15	−90.54	−13.62
Makushin	MK-03F	Glacier valley	08/11/15	−94.79	−13.9
Tana	Tana-02F	East side	08/14/15	−78.59	−12.86

per million (ppm) for CO_2, 0–80 parts per thousand for H_2O], and electrochemical SO_2 (City Technology, Ltd., 2T3STF, 0–100 ppm) and H_2S sensors (City Technology, Ltd., EZT3H, 0–100 ppm). All data were logged at 1 Hz to the MultiGAS datalogger (Campbell Scientific, CR1000) and also displayed in real time using a tablet computer. An ideal gas-type correction for pressure and temperature was applied to the SO_2 and H_2S sensor data, and the raw CO_2 signal was filtered using a digital single-pole recursive low pass filter to better match the H_2S sensor response. Portable calibration gases (3000 ppm CO_2, 10 and 2 ppm SO_2, and 10 and 2 ppm H_2S, all values certified to ±2%) were used to assess sensor responses in the field. The response of the CO_2 instrument was tested 10 times between August 10–20, 2015, and the H_2S sensor was tested 5 times between August 15–20, 2015. Both sensors were observed to be accurate and precise within ≤ 4 percent of the standard values during the field campaign (Werner and others, 2017). We estimate that the total analytical uncertainty for molar CO_2/H_2S ratios in this study is <15 percent at 95 percent confidence.

Makushin Volcano

Makushin Volcano is an active stratovolcano that has erupted in 1995, 1993, 1987, and 1980. Makushin Volcano is listed in the top five highest threat Alaska volcanoes in the National Volcano Early Warning Systems report (Ewert and others 2005, 2018). Geochemical studies of gases and waters from Makushin Volcano are few, and most of what is known about the fluids stems from geothermal prospecting studies that took place in the early 1980s (Motyka and others, 1983; Motyka and others, 1988). Prior to 2015, the most recent published gas data from Makushin Volcano were from samples collected in 1996 (Symonds and others, 2003a, 2003b).

Makushin Volcano hosts an active hydrothermal system that is driven by a shallow magma body that lies beneath the summit region of the volcano (Motyka and others, 1988). Evidence of this magmatic source comes from gas collected at fumaroles that show a clear magmatic signature in helium isotopes (R_C/R_A = 7.85; Motyka and others, 1983). Confirmation of ongoing activity is suggested by visual observations of robust degassing in the summit region made in recent years by crews from the Alaska Volcano Observatory (for example, https://www.facebook.com/USGeologicalSurvey/videos/1133708266675155/). The hydrothermal system is fed by meteoric waters that infiltrate, are heated and ascend in the summit region, and then flow laterally to the east and south of the volcano in a discontinuous envelope of hydrothermal manifestations. Fumaroles, hot springs, and alteration of surface rocks due to hydrothermal activity are extensive in Makushin Valley (to the east) and Glacier valley (an informally named region south of Makushin Volcano and east of Makushin village). The chemical composition of these features varies along the flow path due to water-rock interaction and boiling processes (Motyka and others, 1988).

Three areas were targeted for sampling in 2015 and included the summit, upper Glacier valley (herein after referred to as UGV), and Makushin Valley (fig. 5). The summit was not accessible due to low cloud cover and high winds, and Makushin Valley and the UGV were only accessible to an elevation of ~550 meters (m) and for very brief periods on August 9 and 11, 2015. Sampling targets were guided by the coordinates of sample sites in previous studies (Motyka and others, 1993, Symonds and others, 2003).

Figure 4. Photograph showing typical placement of MultiGAS instrument downwind of fumarole. Christoph Kern is shown here at the informally named mount Finch, a volcanic vent near the center of Fisher Caldera. U.S. Geological Survey photograph by Cynthia Werner.

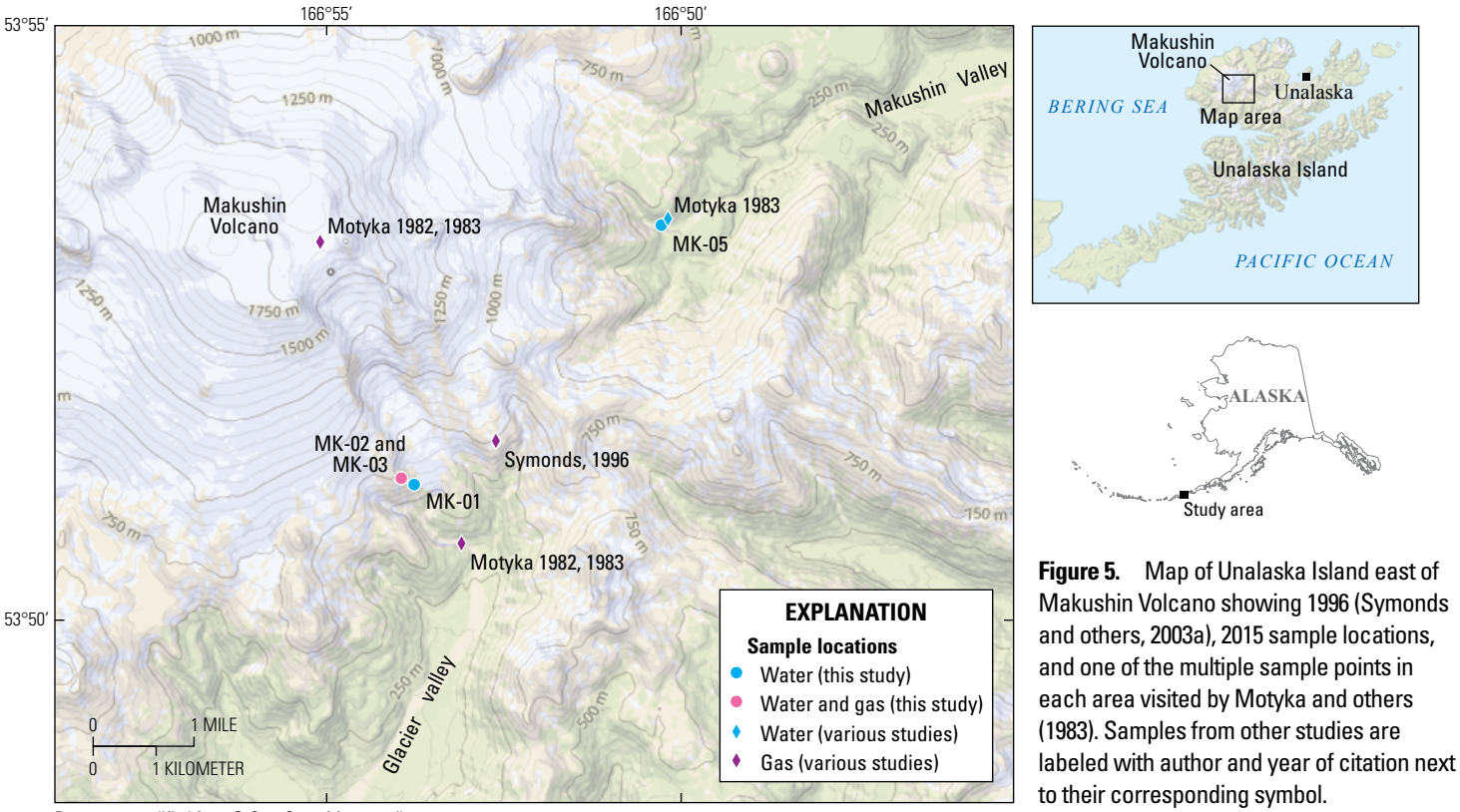

Base maps modified from © OpenStreetMap contributors
Projection: WGS 84 Web Mercator

Figure 5. Map of Unalaska Island east of Makushin Volcano showing 1996 (Symonds and others, 2003a), 2015 sample locations, and one of the multiple sample points in each area visited by Motyka and others (1983). Samples from other studies are labeled with author and year of citation next to their corresponding symbol.

Makushin Valley

We could not locate the fumarole fields in Makushin Valley where Motyka and others (1983) sampled in the 1980s, although the coordinate for his sample was within 300 m of our location (fig. 6). We also did not find a 2,500 m^2 area of thermally altered ground with mud pots and fumaroles as described in Motyka and others (1983), and it is possible that cloud cover inhibited our ability to locate this extensive area. We observed a well head, potentially that of ST-1 drilled in 1983, but there were no obvious thermal springs or fumaroles in the area. One cold pool was sampled in Makushin Valley (fig. 6).

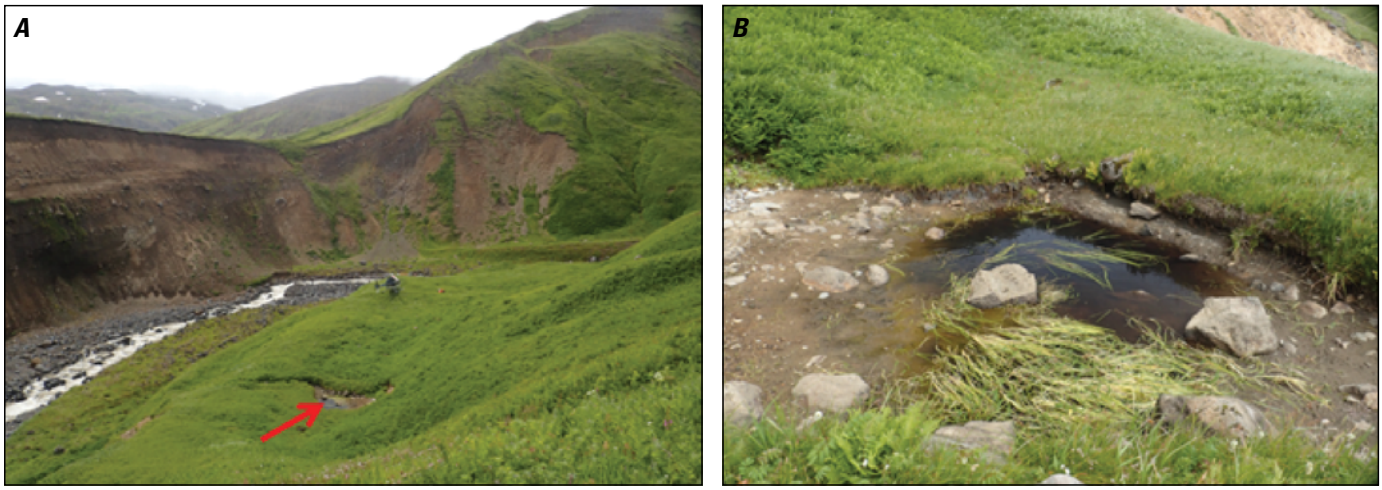

Figure 6. Photographs of the Makushin Valley on Unalaska Island in 2015. *A*, Photograph of Makushin Valley is taken from the north and shows the location of sample MK-05 (red arrow). *B*, Photograph of the pool where sample MK-05 was taken. U.S. Geological Survey photographs by Cynthia Werner.

Glacial Valley

We observed separate areas of thermal manifestations in UGV as described in Motyka and others (1983). Hot springs and fumaroles are located in the eastern and western forks of UGV (fig. 7). We collected samples on the western fork near one of the three main locations where Motyka sampled in the 1980s. However, the majority of samples collected by Motyka and others (1983) and by Symonds and others (2003) were from the eastern fork of the UGV. The fumaroles at this location were not accessible because of the short time window available for sampling, and the western fork was selected as it seemed to be degassing just as vigorously as the eastern fork.

Samples in the western fork of UGV included gas from an area of steaming ground with several fumaroles and minor springs that issued from possible glacial moraine deposits at or near stream level (fig. 8). Temperatures of the fumaroles and hot springs were at or near boiling point (max 100.3 °C). Two springs were sampled for water chemistry (MK-01 and MK-02), one fumarole for gas chemistry (MK-03), and in situ measurements were also collected by the MultiGAS instrument (fig. 8; table 1, 2).

Water Chemistry Summary

Although few water samples were collected, some interesting observations and comparisons can be made with previous data from Makushin Volcano hydrothermal areas. The composition of the early 1980s water samples varied quite dramatically with location, and it was therefore important to identify which of the

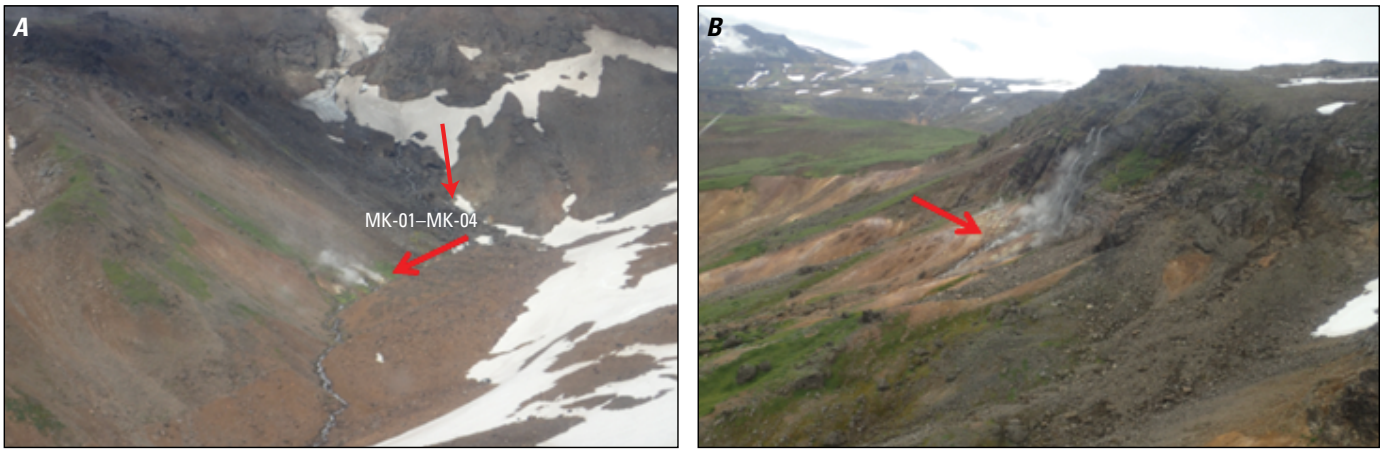

Figure 7. Photographs of the upper Glacier valley's eastern and western fork, southeast of Makushin Volcano. *A*, Photograph the upper Glacier valley's western fork looking northwest to the locations of samples MK-01, MK-02, MK-03, and MK-04. *B*, Photograph of the upper Glacier valley's eastern fork looking south down the valley where Motyka and Symonds sampled in the 1980s and 1996. U.S. Geological Survey photographs by Cynthia Werner.

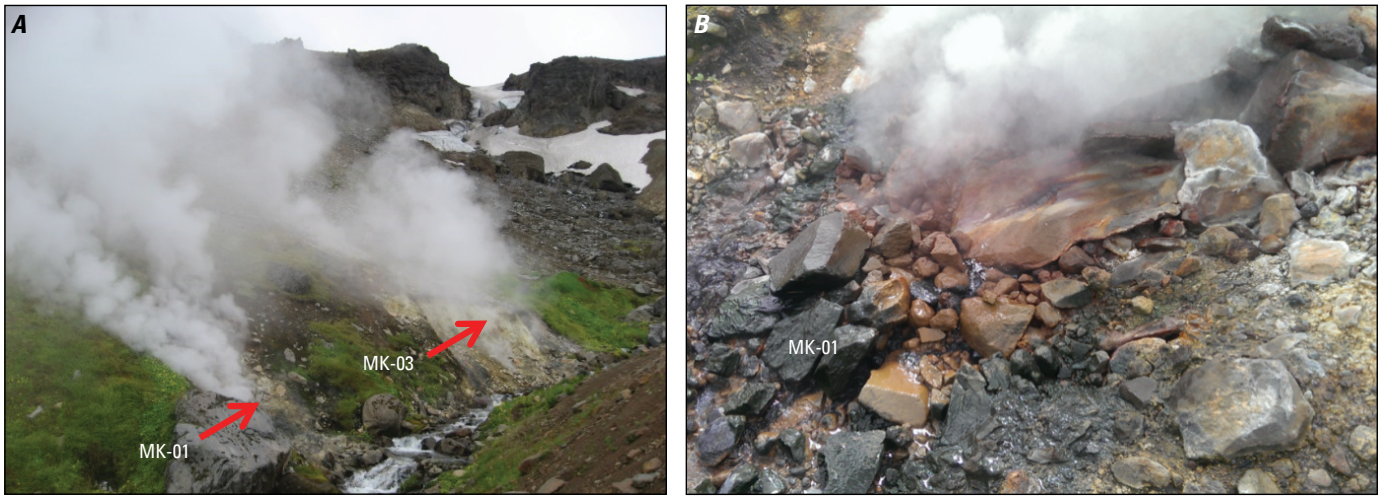

Figure 8. Photographs of the western upper Glacier valley's western fork, southeast of Makushin Volcano, looking south at the two main areas of fumarole and spring output. MK-01 and MK-03 are separated by about 50 meters and their locations are marked by red arrows. Gas (MK-03, 100.3 °C) was sampled from bank of somewhat diffuse output. The most vigorous fumarole and 'geyser-like' hot spring (MK-01, 99 °C) in 2015, is shown in *A* and *B* (*B* showing a close-up of this feature). Gas was not sampled at this fumarole due to concern about air contamination, but a water sample was collected (MK-01). U.S. Geological Survey photographs by Christoph Kern and Cynthia Werner.

samples from previous studies were most likely taken from the western fork where we sampled. Sample MK-05 from Makushin Valley was located very near to fumarole fields 1 and 2 (samples M-a through M-d; Motyka and others, 1983). The 2015 water samples, MK-01 and MK-02, were collected in the western fork of the UGV and are closest to G-l from Motyka and others (1983, 1988). Compositionally the waters are more similar to Motyka's 1982 spring sample G-d2, which is located at the confluence of the eastern and western forks of the UGV.

Stable isotope values (delta deuterium [δD] and oxygen 18 [$\delta^{18}O$]) of the Makushin Volcano springs (fig. 9, table 1) suggest a meteoric water source very similar to many of the water samples taken in the 1980s. The water temperature of the spring where sample MK-02 was collected was 93.6 °C, and the isotope data plot among most of the 1980s water samples and very close to the meteoric trend. In contrast, the temperature of sample MK-01 was 99 °C, and the isotope data of this sample are shifted to the right of the meteoric water line. MK-01 was a low-flow spring associated with a large spattering fumarole, suggesting the shift away from the meteoric water line could be attributed to near-surface boiling and steam loss. A similar finding is observed with the G-d1 sample of Motyka and others (1983), which was 97 °C (fig. 9). This is much hotter than all the other water samples collected by Motyka and others (1983, 1988), thus supporting this interpretation. The isotopic composition of MK-05 is also shifted to the right of the meteoric water line. MK-05 was not flowing and the stable isotope values are apparently affected by evaporative processes (it was apparent the pool was shrinking, fig. 6). Lastly, MK-03 is a fumarolic condensate collected showing the effect of boiling on the gas component.

Overall the compositions of the 2015 water samples were similar in character, but more dilute than those collected in the early 1980s. It should be noted that the water samples collected by Motyka and others (1983) in the eastern fork of UGV, while more numerous, were similar in character to sample G-l collected in the western fork of UGV. As far as the authors are aware, only gas was sampled by Symonds and others, 2003. The 2015 waters were low in chlorine (Cl) and silica (SiO_2), and relatively rich in bicarbonate (HCO_3) and sulfate (SO_4) (fig. 10, table 1). This composition suggests that these springs are not directly associated with the deep hydrothermal system at Makushin Volcano (such as those in lower UGV sampled by Motyka in 1982) and are instead related to condensation of steam in shallow meteoric waters. Most striking is the comparison of SO_4 in

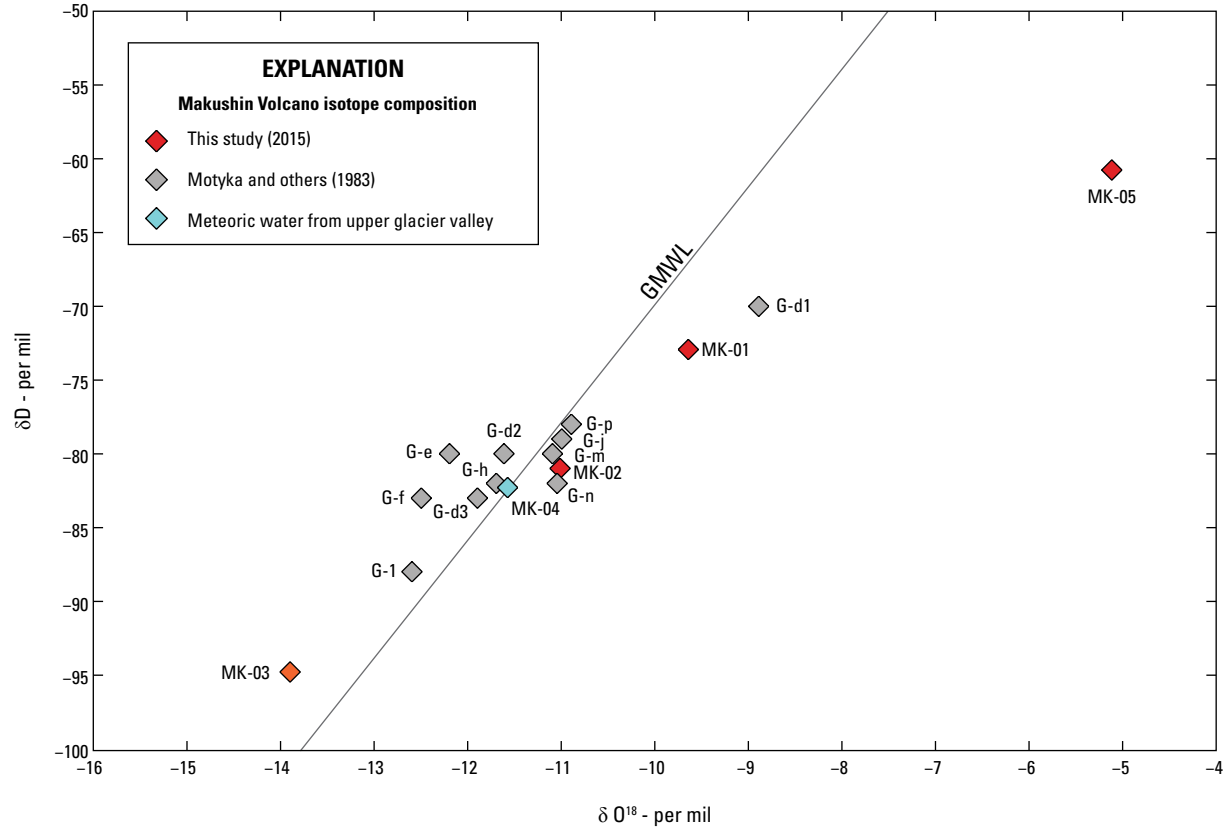

Figure 9. Graph showing the stable isotope composition of thermal waters from the upper Glacier valley (UGV), southeast of Makushin Volcano, from 2015 (red and orange) and the Motyka and others samples from the 1980s (gray). Samples from the 1980s are labeled with G-x (as per the labeling notation in Motyka and others, 1983), and 2015 are labeled by MK-xx. MK-04 (blue) is a meteoric water sample in the UGV and lies on the Global Meteoric Water Line (GMWL), shown in gray. Scatter in the G-x samples has been described in detail by Motyka and others, 1983.

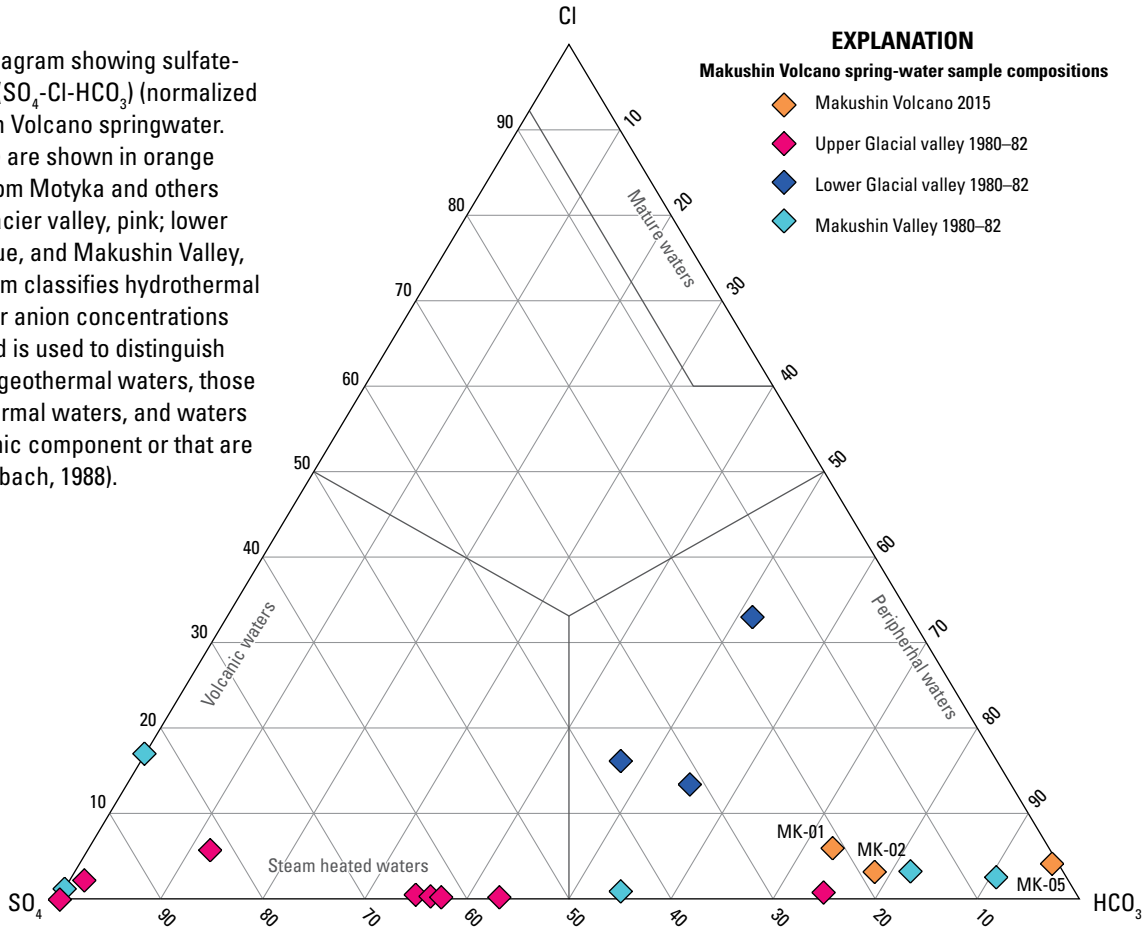

Figure 10. Ternary diagram showing sulfate-chloride-bicarbonate (SO_4-Cl-HCO_3) (normalized by mass) for Makushin Volcano springwater. The 2015 data (MK-xx) are shown in orange along with samples from Motyka and others (1983, 1988) (upper Glacier valley, pink; lower Glacier valley, dark blue, and Makushin Valley, light blue). This diagram classifies hydrothermal waters using the major anion concentrations (Cl, SO_4, and HCO_3) and is used to distinguish the waters as mature geothermal waters, those peripheral to hydrothermal waters, and waters influenced by a volcanic component or that are steam heated (Giggenbach, 1988).

UGV water, which was about 20 times lower in 2015, whereas HCO_3 concentrations were lower only by a factor of 3. In fact, MK-01 and MK-02 were lower in SO_4 than nearly all of the samples collected in the 1980s (fig. 10). Thus, we do not think that the variations could be due to spatial variations. Here SO_4 concentrations are driven by the oxidation of H_2S gas in surface waters (Motyka and others, 1983), thus indicating most likely a relatively lower flux of steam and gas in 2015. All but one of the 1980s UGV water samples plotted in the 'steam heated water' section of the SO_4-Cl-HCO_3 ternary diagram (fig. 10), whereas the 2015 samples plot in 'peripheral waters' area, demonstrating an overall increase in HCO_3 relative to SO_4 or Cl (fig. 10). Compared to the water samples of other Aleutian Islands from 2015, the Makushin Volcano water samples were richer in HCO_3 than any other location and were most similar to springs in Fisher Caldera. These findings are consistent with a change in volcanic activity at Makushin volcano between 1983 and 2015. The 1982 samples were collected shortly following the 1980 eruption when there could have been more heat and gas available from degassing of the shallow magma. Alternatively, there could have been considerably less hydrothermal upflow in 2015 relative to the 1980s (further discussion at the end of the section).

Cation concentrations in the waters from both years contain calcium (Ca)> sodium (Na)> magnesium (Mg)> potassium (K). Concentrations of Ca, Na, and K were lower by factors of 10, nearly 5, and 2, respectively, in 2015 relative to 1982. Mg was low in both sampling periods. SiO_2 concentrations were also lower in 2015, dropping from 135 to 60 milligrams per liter (mg/l). We suggest the drop in the anion and cation concentrations could perhaps be due to a decrease in the output of the hydrothermal fluid component over the interval between the 1980s and 2015.

Geothermometry calculations based on water chemistry were not performed as they are only suitable for waters that are in equilibrium with the underlying rocks. Immature waters that are not in equilibrium, such as those described here, are not suitable for geothermometry.

Gas Chemistry Summary

The gas sample collected in UGV contained some air demonstrated by concentrations of oxygen (O_2) as much as ~1.5 percent, and molecular nitrogen to argon (N_2/Ar), and N_2/O_2 ratios similar to that of air (fig. 11). These ratios were shifted slightly toward the magmatic component from an air composition, similar to the data collected in the 1980s (fig. 11). The primary components were CO_2 and H_2S (table 2). Thus, the gas is hydrothermal in character, which is consistent with previous

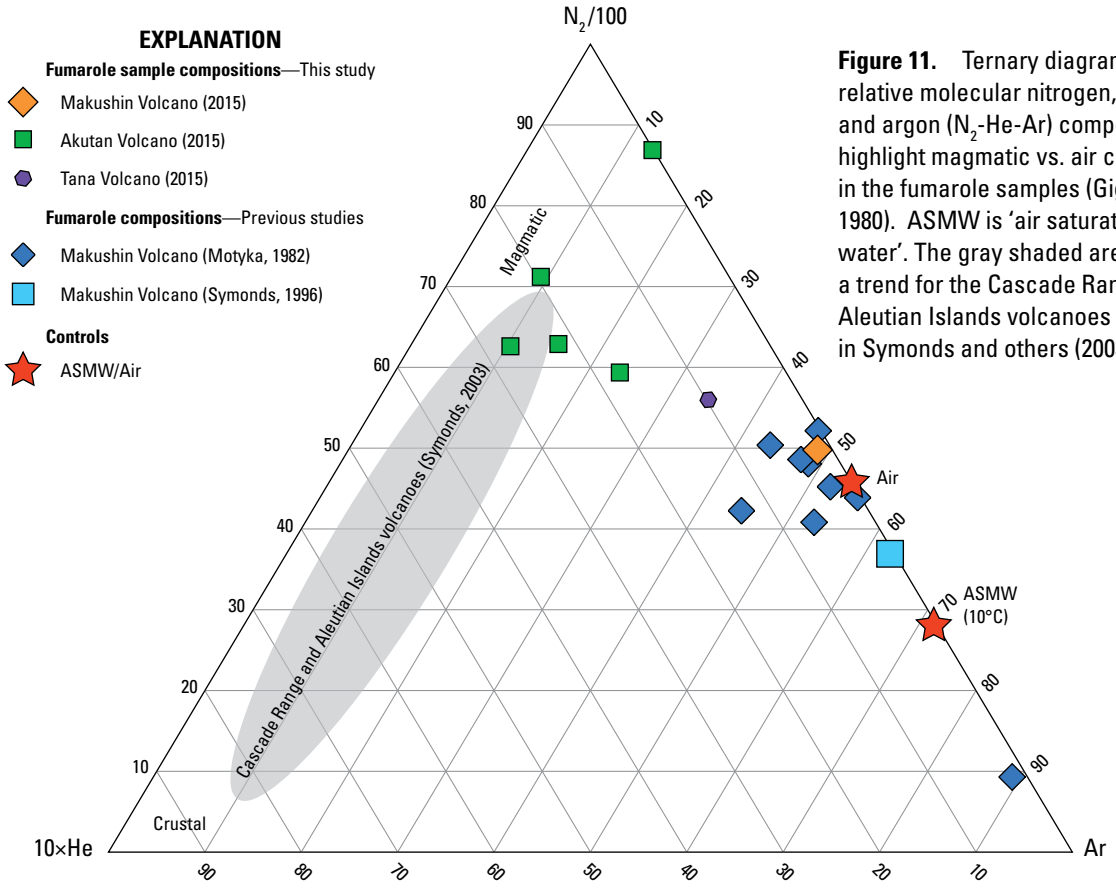

Figure 11. Ternary diagram showing relative molecular nitrogen, helium, and argon (N_2-He-Ar) compositions to highlight magmatic vs. air contribution in the fumarole samples (Giggenbach, 1980). ASMW is 'air saturated meteoric water'. The gray shaded area represents a trend for the Cascade Range and Aleutian Islands volcanoes as presented in Symonds and others (2003).

sampling of gases at Makushin Volcano, including a superheated fumarole in 1982. Whereas Motyka and others (1983) sampled the summit fumarole, this area was not accessible in 2015 due to cloud cover and high winds. Thus, it is unclear if the summit area was emitting any SO_2 in 2015, and it is also not clear if procedures to analyze for SO_2 were in place in the 1980s.

The most 'magmatic' (characterized by the lowest CO_2/H_2S) gas sample collected by Motyka and others (1983) was from a superheated fumarole in UGV and had a CO_2/H_2S ratio of 8, compared with gas from the summit area that had a CO_2/H_2S ratio of 15. The data reported by Symonds and others (2003) give a CO_2/H_2S ratio of 10 for a boiling point fumarole in UGV. The ratio in the 2015 UGV fumarole sample was ~ 30, much higher than in the past, but well within the range of CO_2/H_2S ratios at many volcanoes in the Cascades and Aleutians (5–300, Symonds and others, 2003). The MultiGAS-measured CO_2/H_2S was about 50 (fig. 12), higher than that of the fumarole gas, which is likely due to the instrument being placed in a location that had contributions of CO_2 from diffuse sources near the fumarole (the MultiGAS instrument was placed about 2–3 m from the fumarole).

The relative abundances of molecular nitrogen, helium, and argon (N_2-He-Ar) in the 2015 gas are similar to that found by Motyka and others (1983) and Symonds and others (2003) (fig. 12). The data plot off of the Cascade Range–Aleutian Islands arc trend described by Symonds and others (2003) that largely represents various amounts of crustal vs. magmatic input. The Makushin Volcano samples lie between magmatic and air endmembers but are closer to the air endmember.

Carbon and Helium Isotopes

The $\delta^{13}C\text{-}CO_2$ value for the fumarole in UGV (MK-03) is −12.6 per mil, and is consistent with some of the values reported by Motyka and others (1983) (between -10.24 ± 0.3 and −12.96, where the spread in these values was speculated to be because of discrepancies between lab results). These values are all considerably lighter than the UGV sample from 1996, where $\delta^{13}C\text{-}CO_2$ was reported as −7.6 per mil (Symonds and others, 2003). The summit fumarole had a value of −10 per mil in 1982 (Motyka and others, 1988).

The R_C/R_A value for MK-03 (3.76) is lower than what was reported for UGV by Motyka and others (1983) ($R_C/R_A = 4.5$) and by Symonds and others (2003) ($R_C/R_A = 4.81$). They found the most primitive helium isotopes at the summit fumarole ($R_C/R_A = 7.83$) and suggested that varying amounts of crustal components led to the wide variation in R_C/R_A observed across the hydrothermal area. The reduction in R_C/R_A values since previous studies is consistent with the other geochemical findings that

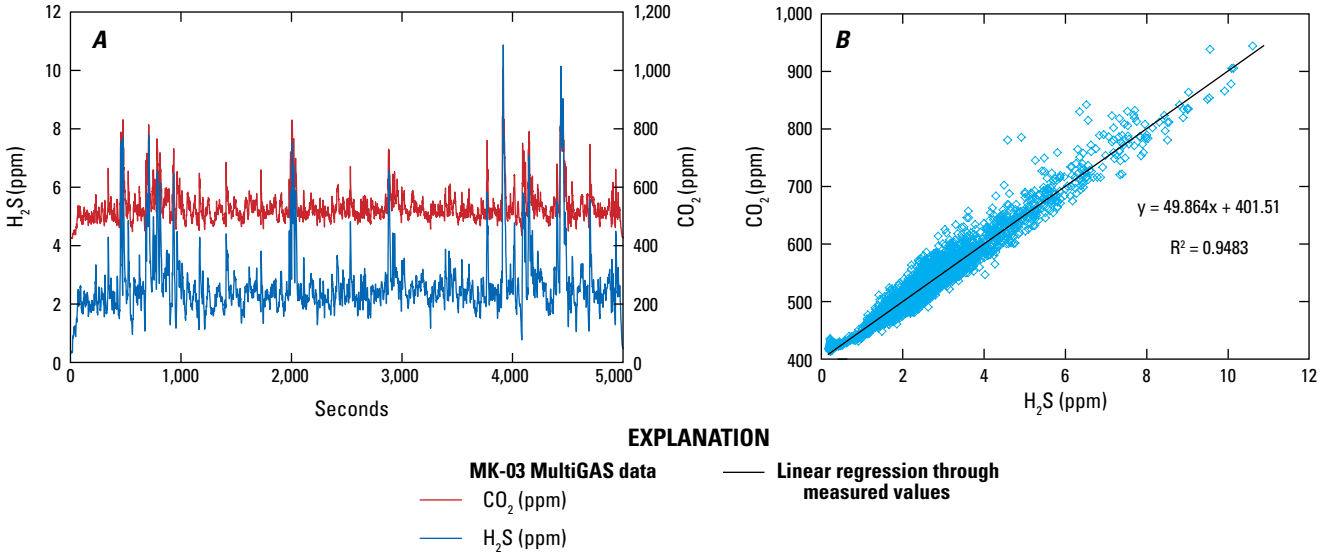

Figure 12. Graphs showing MultiGAS data collected near MK-03 on August 11, 2015. See figure 5 for location. *A*, Time series graph of the CO_2 and H_2S data collected on site (one reading per second). *B*, Graph displaying the regression of CO_2 to H_2S. Good correlation is observed between CO_2 and H_2S. CO_2/H_2S based on these data is about 50. Values are given in parts per million (ppm).

suggest weaker hydrothermal discharge at the surface in 2015, thus resulting in a more dominant crustal He signature.

Gas Geothermometry

Application of the D'Amore and Panichi (1980) gas geothermometer to the 2015 sample from UGV (MK-03) gives a temperature of 297 °C, which is identical to the preferred temperature reported by Motyka and others (1983) using the same geothermometer (ranged from 230–297 °C, with 297 °C reported for the high-pressure superheated fumarole in UGV).

Apparent Decline in Hydrothermal Activity at Makushin Volcano since the 1980s

Several observations have been made that suggest the magmatic/hydrothermal component of the surface thermal features on the flanks of Makushin Volcano have greatly declined since the early 1980s when these features were studied and sampled by Motyka and others (1983, 1988). The waters collected in the UGV (MK-01 and MK-02) were substantially diluted compared to previous samples collected in this location by Motyka and others (1983, 1988). The large drop in SO_4 in combination with the notable increase in CO_2/H_2S in the fumarolic gases suggests that hydrothermal influence has waned in the UGV area. Minor decreases in the helium isotopic ratio also provide additional support for declining magmatic output.

Motyka and others (1988) used several sources of data and observation (for example, hot spring deposits, fluid inclusions, and drill core mineralogy) to suggest that the hydrothermal system had been active for thousands of years. In addition, well ST-1 produced 193 °C water throughout a 45-day flow test in 1984, which helped define the existence of a large-scale reservoir. Thus, the apparent decline in the vigor and hydrothermal characteristics of the surface features over the past three decades may reflect shrinkage or cooling of a large and long-lived reservoir or may result from a decline in upflow between the reservoir and the surface. Upflow in 1981–1982 could have been temporarily increased as a result of changes to permeability because of the eruption in 1980. Thus, the decline we observed ~20 years following the last eruption in 1995 could be ascribed to gradual mineral sealing in the fluid flow paths or to redirection of flow paths that deprive the upper elevation features of fluids.

The apparent decline in hydrothermal discharge at Makushin Volcano is analogous, but opposite, to the striking increase in hydrothermal discharge observed on Akutan Island in the past several decades (see Bergfeld and others (2013) and discussion in next section). The increased discharge of Akutan hydrothermal waters was tentatively attributed to an increase in permeability of the thermal aquifer in response to a seismic crisis in 1996. Potential linkages between hydrothermal discharge and volcano/tectonic unrest at Aleutian Islands arc volcanoes may be more common than currently thought but are poorly constrained due to the infrequency of sampling expeditions. Opportunities clearly exist here for process-oriented research on these linkages.

Future Study Recommendations

Future studies for volcano hazards monitoring should focus on the summit region of Makushin Volcano. Motyka and others (1983) observed a magmatic He isotopic signature for

gases at the summit. Resampling of this area would provide an understanding if these values have changed over time. It would be important to determine if SO_2, H_2S, or a combination of the two gases is emitted from the summit region in order to determine the major gas geochemistry and the CO_2/S_T and SO_2/S_T ratios of the summit emissions (here S_T refers to the combined sulfur from SO_2 and H_2S). These ratios would help provide an understanding of whether the summit is emitting gases that are more or less hydrothermal in nature than the gases sampled in this study.

Should the summit remain inaccessible, it would be advisable to continue to sample the springs in the upper reaches of UGV. This would be done in order to determine SO_4 and Cl concentrations to test if higher values are associated with periods of higher heat output coincident with or following volcanic unrest. Increases in these components would shift the plot of water samples on a HCO_3-SO_4-Cl ternary diagram from the 'peripheral' water region (fig. 10) and likely back into the 'steam-heated' and possibly even 'volcanic waters' region should any Cl be discharged.

Akutan Volcano

Akutan Volcano is an active stratovolcano that last erupted in 1992 and is listed second among all Alaskan volcanoes in terms of threat in the National Volcano Early Warning Systems report (Ewert and others, 2005, 2018) (fig.13). Akutan Volcano hosts an active hydrothermal system driven by recent volcanic and magmatic activity. The Akutan hydrothermal system has been extensively studied in recent years (Bergfeld and others, 2014; Stelling and others, 2015). The data from these studies support original conceptual models of a hydrothermal system, where a reservoir lies beneath an active fumarolic area (figs. 13 and 14) on the eastern flank approximately 3 kilometers (km) from the active cone. Meteoric water enters the system at higher elevations and is heated along its flowpath by an underlying magmatic intrusion. Gases emit in the fumarolic area on the eastern flank above the upflow zone of the hydrothermal system and waters flow laterally east to Hot Springs creek, an informally named stream that flows into Hot Springs Bay from the southwest.

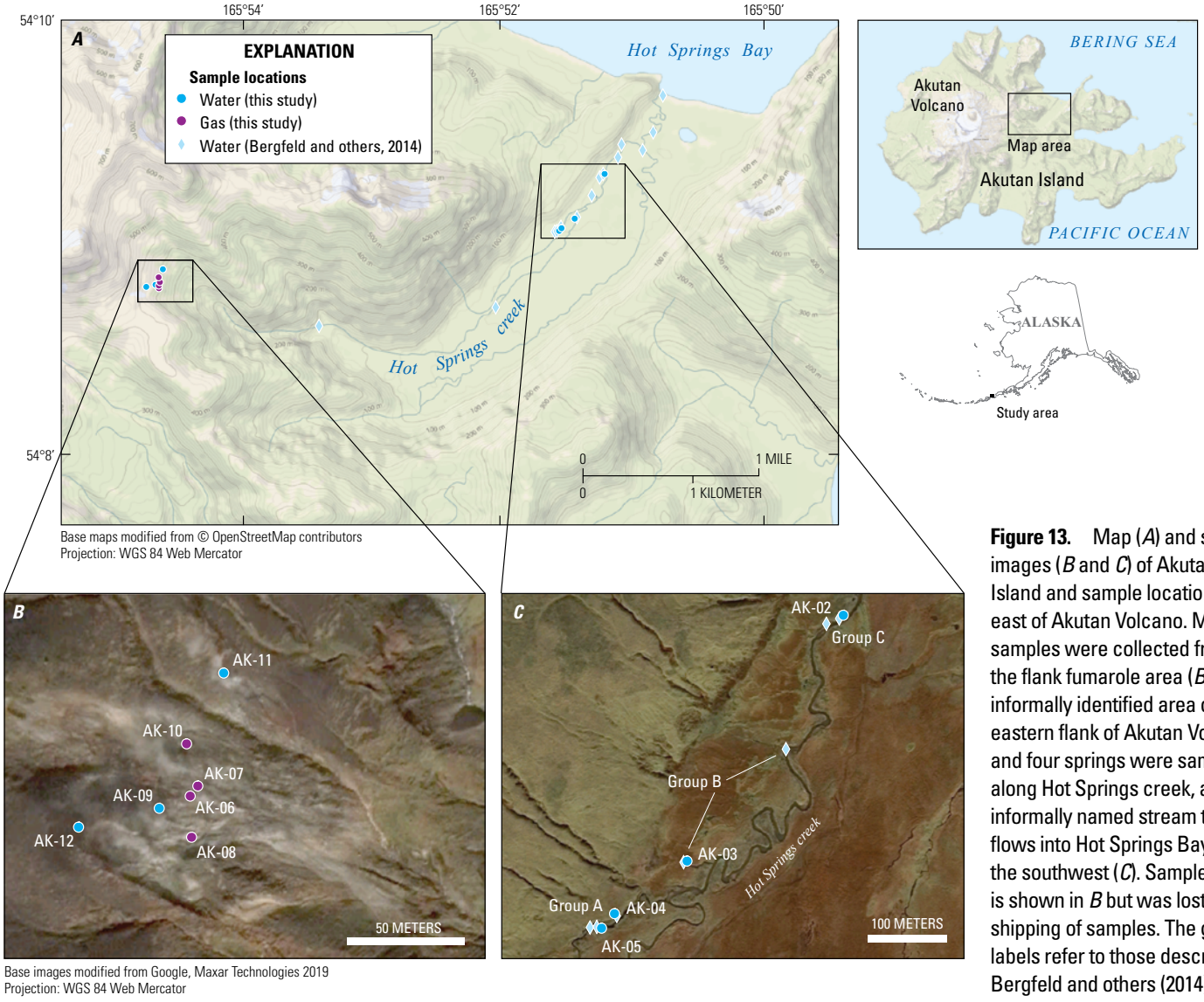

Figure 13. Map (*A*) and satellite images (*B* and *C*) of Akutan Island and sample locations east of Akutan Volcano. Most samples were collected from the flank fumarole area (*B*), an informally identified area on the eastern flank of Akutan Volcano; and four springs were sampled along Hot Springs creek, an informally named stream that flows into Hot Springs Bay from the southwest (*C*). Sample AK-10 is shown in *B* but was lost in shipping of samples. The group labels refer to those described in Bergfeld and others (2014).

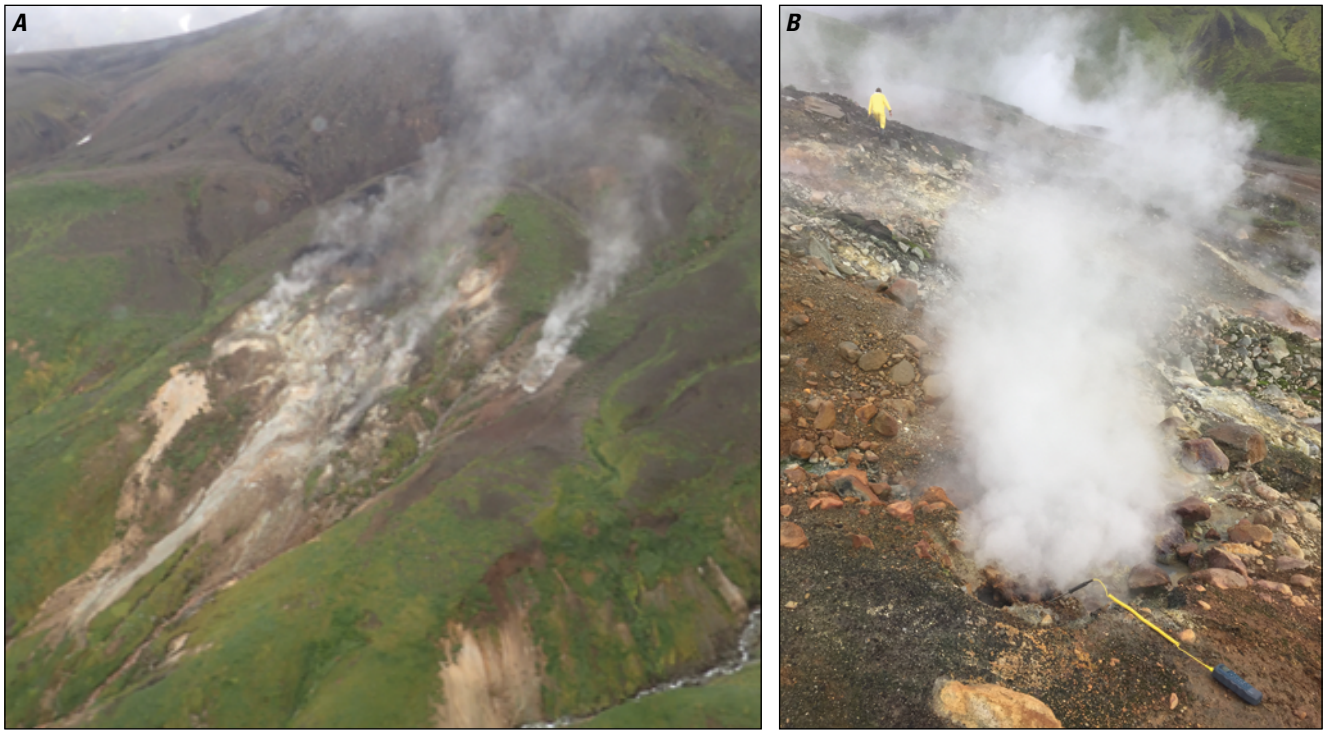

Figure 14. Aerial and ground-based photographs of the flank fumarole area, an informally identified area on the eastern flank of Akutan Volcano that hosts fumarolic and diffuse gas discharge and the headwaters of Hot Springs creek (see figure 13 for location). The scale of the area shown in *A* is approximately 500 meters across and is looking northwest up the valley. *B*, Ground-based photograph of the flank fumarole area, looking to the north. U.S. Geological Survey photographs by Cynthia Werner.

Multiple areas of steam and gas emission were visually observed on the summit cone (fig. 15), but no volcanic gas was detected during airborne traverses around the summit area on August 18, 2015. Several orbits around the summit cone were made during calm and clear conditions. Unfortunately, the summit could not be visited on the ground due to helicopter scheduling with other field crews.

Sampling took place in the area of fumarolic and diffuse gas discharge in the upper reaches of the valley that hosts the headwaters of Hot Springs creek, which runs into Hot Springs Bay (herein after referred to as the flank fumarole area) and at the springs that issue along Hot Springs creek on August 17 and 21, 2015 (fig. 13). Sampling was focused on the hottest features in the flank fumarole area (here bottles filled so quickly we thought they were air contaminated) and on several of the features previously sampled along Hot Springs creek (Bergfeld and others, 2014).

Water Chemistry Summary

Consistent with the findings of Bergfeld and others (2014), the stable isotope values of waters along Hot Springs creek plot clustered and shifted about 1–2 per mil to the right of the Global Meteoric Water Line (GMWL) with no increase in δD, suggestive of a shift in isotope composition due to water-rock interaction (fig. 16). Water samples collected in the flank fumarole area (AK-09 and AK-11) plot considerably off of the GMWL and are likely affected by surface evaporation.

The compositions of the springs in the Hot Springs creek area have analyte concentrations that are consistent with the range of values reported by Bergfeld and others (2014) (fig. 17), whereas 2015 water samples from the flank fumarole area were low in Cl (table 1). The lack of Cl demonstrates that no appreciable deep hydrothermal water issues in this area, and high SO_4 values reflect the oxidation of H_2S in shallow groundwaters. In terms of SO_4-HCO_3-Cl, waters from the springs in Hot Springs creek on Akutan Island are the most mature (highest in Cl) of any we sampled in the Aleutian Islands (fig. 18), and the chemistry of the waters is nearly identical to that presented in Bergfeld and others (2014) and Stelling and others (2015) (not shown).

Fluid Geothermometry

Several springs sampled from the Hot Springs creek area are suitable for the use of fluid geothermometers. The data here suggest that samples AK-04 and AK-02 are in partial equilibrium with estimated temperatures of approximately 210–220 °C (fig. 19). The equilibrium temperatures are similar to the results presented for the Hot Springs creek area (Bergfeld and others, 2014; Stelling and others, 2015), which might be expected given the similarity in the chemistry of the samples (fig. 19).

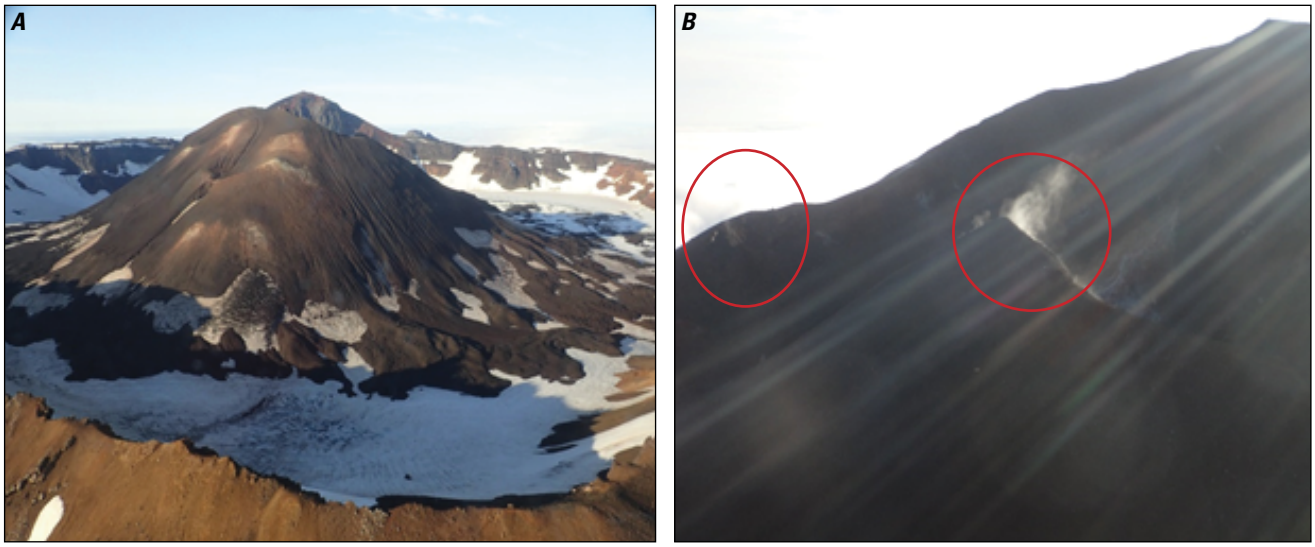

Figure 15. Photographs of Akutan Volcano summit caldera and cone on August 18, 2015. *A*, The roughly 1-km wide summit cone shows multiple areas of alteration and indicate current and (or) past magmatic gas emission. The cone sits in the approximately 2.5 km wide caldera and this image is from the west looking east. *B*, Isolated steam vents were visible when backlit from the sun on the south side of the cone. U.S. Geological Survey photographs by Cynthia Werner.

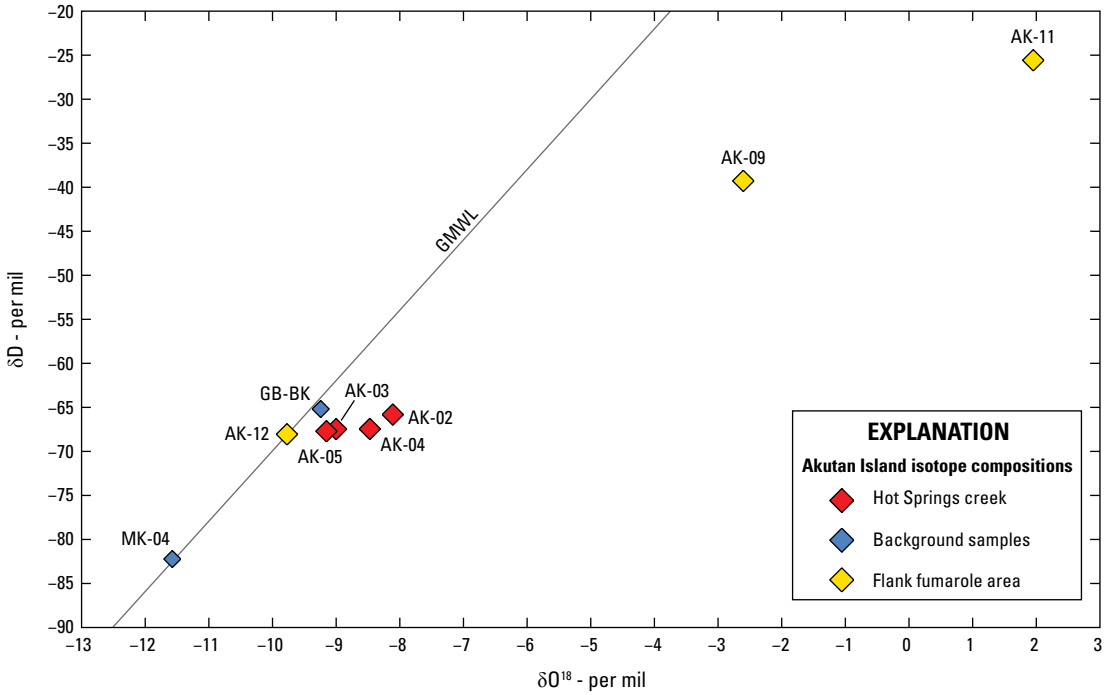

Figure 16. Graph displaying stable isotope data for water samples collected from hydrothermal areas on Akutan Island in 2015. AK-09 and 11 are from acidic springs with low flow in the flank fumarole area, an informally identified area on the eastern flank of Akutan Volcano on Akutan Island. MK-04 and GB-BK are background samples that plot on the Global Meteoric Water Line (GMWL).

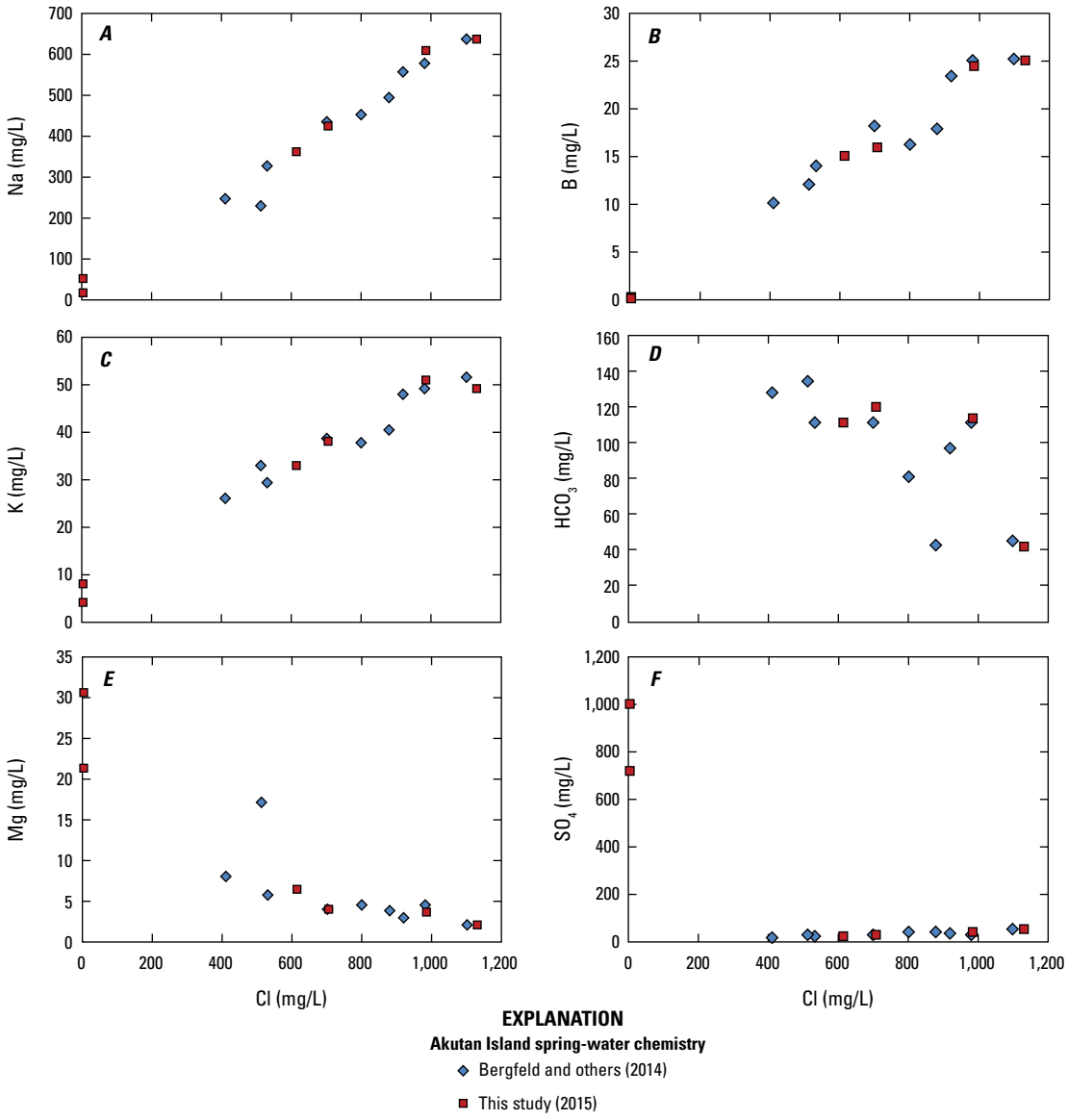

Figure 17. Scatterplot diagrams (*A–F*) showing the constituent concentrations vs. chlorine (Cl) for thermal springwaters from 2015 (red squares) and 2010 (blue diamonds, from Bergfeld and others, 2014) sampled in the Hot Springs creek area on Akutan Island (figure 13). Springwater chemistry shows consistent results between the two years. The low Cl, high SO_4 samples from 2015 (*F*) are waters from low-flow springs in the flank fumarole area, an informally identified area on the eastern flank of Akutan Volcano on Akutan Island. Values are given in milligrams per liter (mg/L).

Gas Chemistry Summary

The 2015 gas samples from the flank fumarole area are high in CO_2 and H_2S, with minor amounts of CH_4, and are hydrothermal in character, consistent with previous sampling of gases at Akutan Volcano (table 2). The relative abundances of N_2-He-Ar (fig. 12) are nearly identical to those observed by previous studies (Motyka and Nye, 1988; Symonds and others, 2003; Bergfeld and others, 2014, and Stelling and others, 2015), and are typical of arc-type gases with N_2/Ar ratios > 200 (Symonds and others, 2003).

The CO_2/H_2S ratio of all the gas samples from the flank fumarole area were between 45–48, which is consistent with previous measurements (Bergfeld and others, 2014; Symonds and others, 2003). These values are slightly lower than that measured by the MultiGAS instrument (57, fig. 20), which is likely because of an increased sampling of soil degassing with MultiGAS that would be enriched in CO_2 over H_2S. Elevated gas concentrations were measured with the MultiGAS instrument across the flank fumarole area (as much as 500 ppm CO_2 above background, fig 20), which differed from Hot Springs valley, where very low gas concentrations were measured (only 20 ppm CO_2 above background). Here the CO_2/H_2S ratio was 386 (fig. 21), which reflects the preferential scrubbing of H_2S gas in hydrothermal waters compared to CO_2.

Although the summit was not sampled in 2015, it is interesting to note that the CO_2/H_2S measured in 1996 (14.3) by Symonds and others (2003) lies midrange to what was measured in 2012 (7-21) by Bergfeld and others (2014), despite the issues with air infiltration (discussed below). Thus, the differences in CO_2/H_2S between the summit area and that of the flank fumarole area highlight the scrubbing processes in the flank fumarole area, which were much more effective than at the summit.

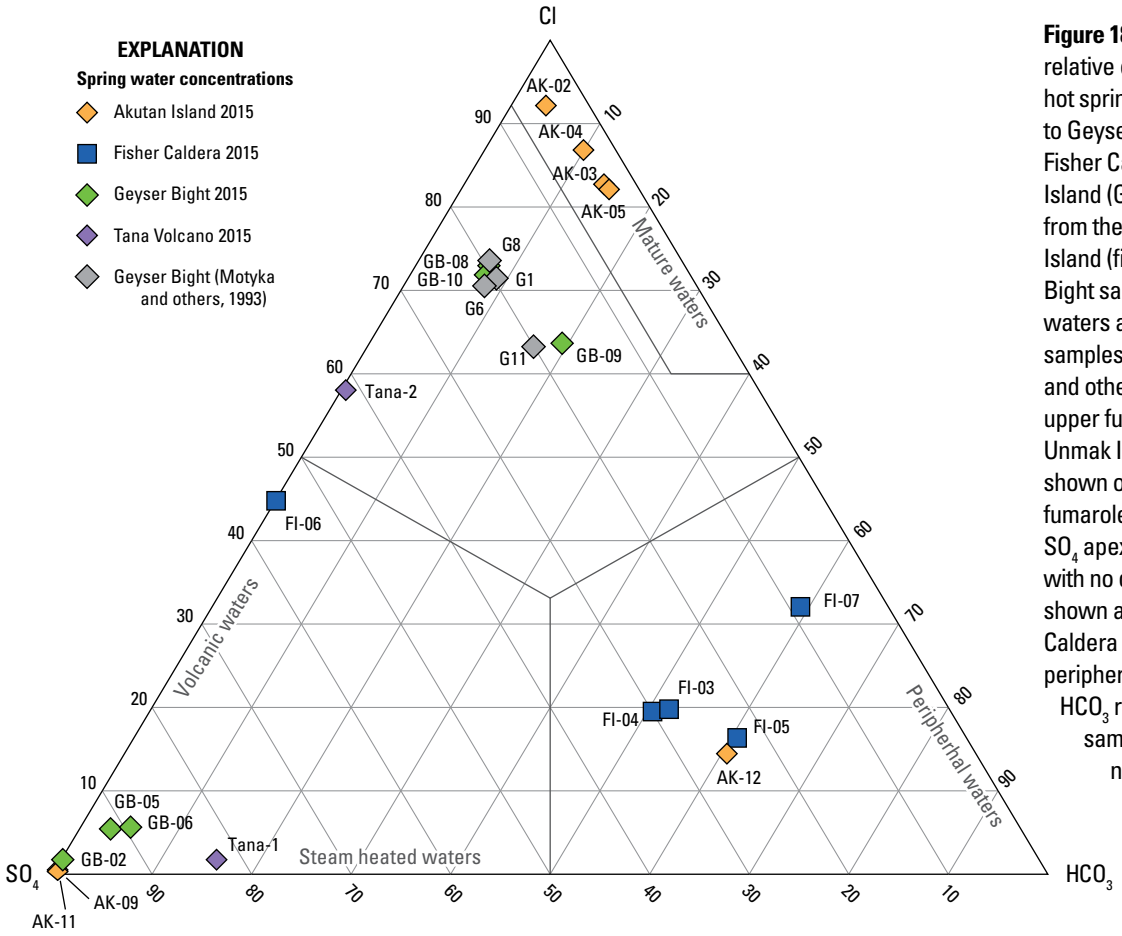

Figure 18. Ternary diagram showing the relative concentrations of SO_4-HCO_3-Cl in hot springs on Akutan Island in comparison to Geyser Bight on Umnak Island and the Fisher Caldera hydrothermal area on Unimak Island (Giggenbach, 1989). Water samples from the Hot Spring creek area of Akutan Island (fig. 13) plot as mature waters. Geyser Bight samples plot just outside of the mature waters area and are nearly identical to samples collected during the 1980s (Motyka and others, 1993). Samples collected in the upper fumarole area of Geyser Bight on Unmak Island (F1 of Nye and others, 1992 shown on fig. 36) and those from the flank fumarole area on Akutan Island plot near the SO_4 apex representing steam heated waters with no deep hydrothermal component. Also shown are the water samples from the Fisher Caldera area. These samples all plot in the peripheral area of the ternary plot with higher HCO_3 relative to other areas, except for the sample from mount Finch, an informally named feature near the central area of Fisher Caldera, which is the only sample to plot in the volcanic waters area of the diagram.

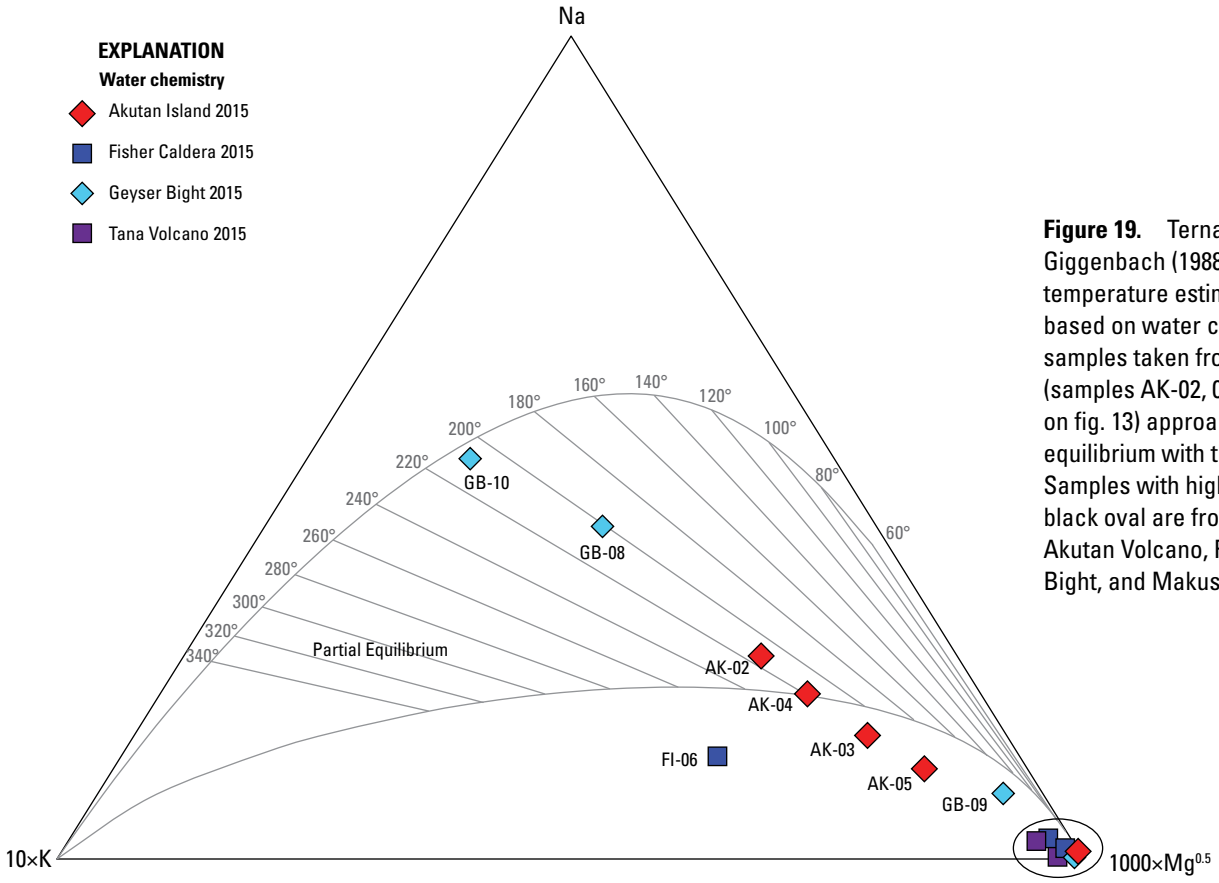

Figure 19. Ternary diagram after Giggenbach (1988) showing reservoir temperature estimates in degrees Celsius based on water chemistry. Akutan Island samples taken from the Hot Springs creek (samples AK-02, 03, 04, and 05 shown on fig. 13) approach or are in partial equilibrium with the underlying rocks. Samples with high Mg contents in the black oval are from various locations at Akutan Volcano, Fisher Caldera, Geyser Bight, and Makushin Volcano.

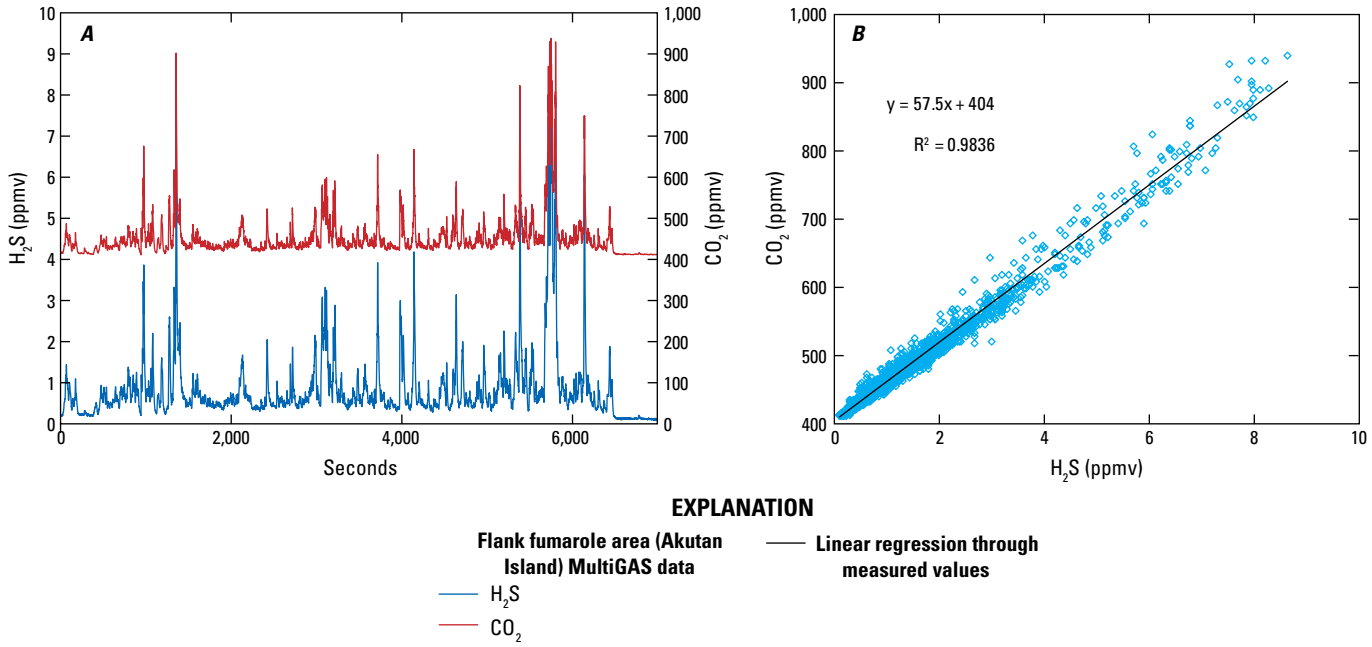

Figure 20. Graphs showing MultiGAS data from the flank fumarole area, an informally identified area on the eastern flank of Akutan Volcano on Akutan Island. (fig. 13). *A*, Time series graph of the data with the peaks of CO_2 and H_2S in parts per million by volume (ppmv) corresponding in time. *B*, Graph displaying the regression of CO_2 to H_2S. Good correlation is observed between CO_2 and H_2S. The CO_2/H_2S based on these data is about 57. Values are given in parts per million by volume (ppmv).

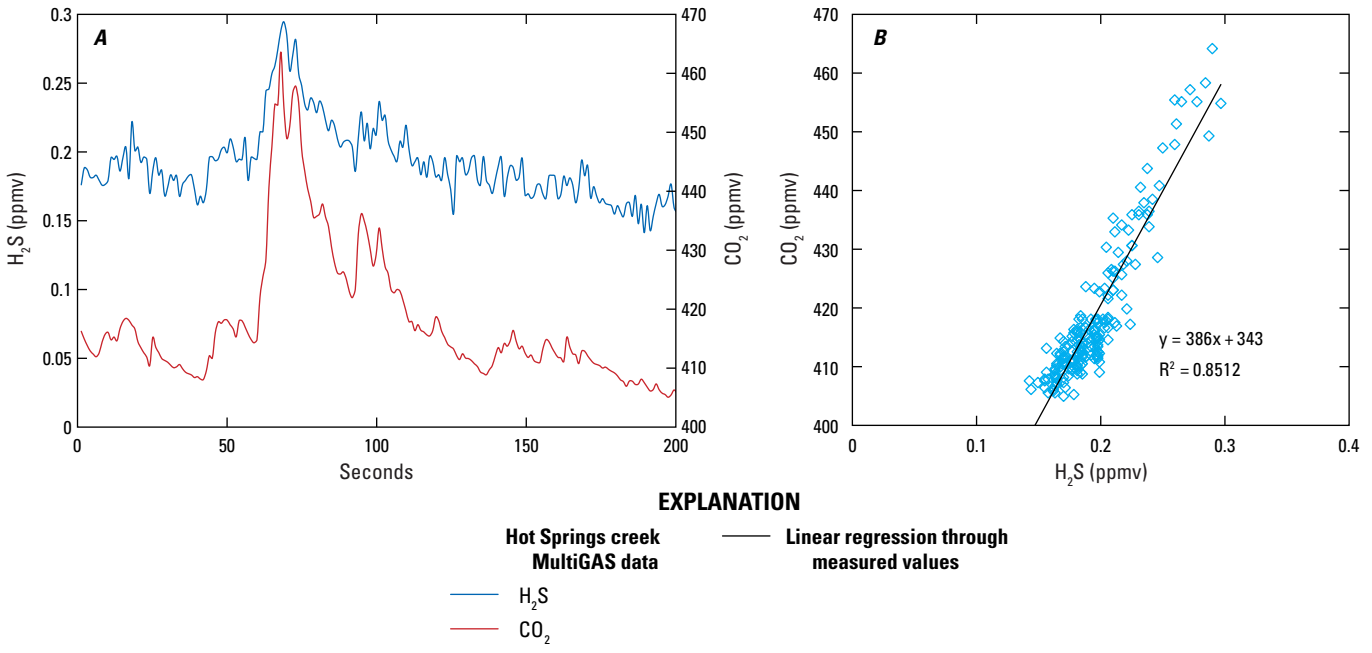

Figure 21. Graphs showing MultiGAS data from the Hot Springs creek area of northwest Akutan Island (fig. 13). *A*, Time series graph of the data with the peaks of CO_2 and H_2S in parts per million by volume (ppmv) corresponding in time. *B*, Graph displaying the regression of CO_2 to H_2S. Reasonable correlation was observed between CO_2 and H_2S for a small subset of the data, but overall concentrations were low. The CO_2/H_2S based on these data is about 386. Values are given in parts per million by volume (ppmv).

Carbon and Helium Isotopes

The average $\delta^{13}C–CO_2$ value for the fumaroles in the flank fumarole area on Akutan Volcano was −10.7 (±0.11) per mil and is consistent with the values reported by Evans and others (2015) for the flank area (−10.6 per mil) but heavier than that of the summit value (−12.4 per mil). These values are more depleted than the sample from 1996 where $\delta^{13}C–CO_2$ was reported as −9.7 per mil for the flank fumarole area (Symonds and others, 2003).

Unfortunately, the two samples collected for helium isotopes from Akutan Volcano in 2015 (AK-06 and AK-10) were air contaminated and lost in shipment, respectively. Bergfeld and others (2014) showed that the most magmatic samples (that is those with the highest R_C/R_A) collected in 2012 were those from the flank fumarole area with R_C/R_A of 7.6, whereas both the summit and Hot Springs creek area had lower values (< 3.8 and < 6.88, respectively). Symonds and others (2003) obtained samples from the summit and the flank fumarole area that were both close (7.23 and 7.25, respectively) to that sampled by Bergfeld and others (2014) in 2012.

Gas Geothermometry

Application of the D'Amore and Panichi (1980) gas geothermometer to the 2015 gas data from the flank fumarole area suggests a reservoir temperature between 238 and 242 °C. These values are consistent with the highest temperatures (236 °C) reported by Bergfeld and others (2014) using the same geothermometer.

Future Study Recommendations

Future studies concerned about volcano hazards monitoring of Akutan Volcano should focus on gas sampling in the summit and flank fumarole area, and specifically on filling in the gaps of this study with regard to He isotopes and continued use of the MultiGAS instrument as a monitoring tool. Because of the changes in isotopic values (C and He) observed between the 1996 sampling (Symonds and others, 2003) and that of 2012 and 2015 (Bergfeld and others, 2014, and this study), it is reasonable to suggest that the summit area was more strongly influenced by shallow magmatic processes in 1996 than in recent years. It is likely that more magmatic signatures were observed because of the eruption in 1992 and seismic unrest in 1996, just several months prior to the sampling of Symonds and others (2003).

As discussed by Bergfeld and others (2014), the summit and the flank fumarole area share a common deep magmatic source, thus both likely present reasonable targets for geochemical monitoring. Bergfeld and others (2014) documented the effect of deep infiltration of air into summit fumarole area samples, thus diluting magmatic gas components and making the flank area a better target in this regard. If accessible, it would be interesting to continue to monitor the R_C/R_A in the summit region to test if the value increases during periods of heightened activity. R_C/R_A values dropped from the 1996 sampling (7.23) to a much lower value in 2012 (3.8). Thus, monitoring the He isotopic value with time at Akutan Volcano might lead to a better understanding of intrusive activity at the volcano.

Because the hydrothermal reservoir lies between the magmatic source and the flank fumarole area, it would be advisable to continue to make measurements in the summit area, given that some species can react with subsurface fluids. In particular, monitoring the C/S ratio and any change in sulfur speciation from H_2S to SO_2 is recommended. Magmatic SO_2 has not been documented in the summit region, and an appearance of SO_2 would indicate a heightened level of activity at the volcano. The MultiGAS instrument provided reasonable correspondence of the CO_2/H_2S ratio with the fumarole samples in the flank fumarole area and should be utilized in future monitoring expeditions to the area because of its ease of use.

Tana Volcano

Tana volcano lies to the east of Mount Cleveland volcano on the remote Chuginadak Island in the Islands of Four Mountains in the central Aleutians Islands, Alaska (fig. 22). The last volcanic activity occurred in the Holocene and there were no reports of thermal activity on the island until 2014 (Evans and others, 2015). Two main areas of thermal manifestation are known to exist on the island; one area is located on the north flank of the volcano and the other near sea level on the eastern side of the volcano near the summit crater lake (fig. 22). In 2014 and 2015 the springs were sampled at both locations (Evans and others, 2015). Gas was sampled on the east coast in 2015, and the MultiGAS instrument was run at both locations.

Temperatures of the features on both the north and east sides of Tana volcano (fumaroles/bubbling springs and hot springs) were below boiling (max 95.8 °C). Sites on the north side mostly consisted of steaming ground with several fumaroles (fig. 23). Minor and low-flow springs issued from where fumaroles emerged out of what appeared to be altered volcaniclastic material. The springwater (Tana-1) was gray because of suspension of clay. Gas and water were collected from one bubbling spring on the eastern side of Tana volcano (Tana-2, fig. 24).

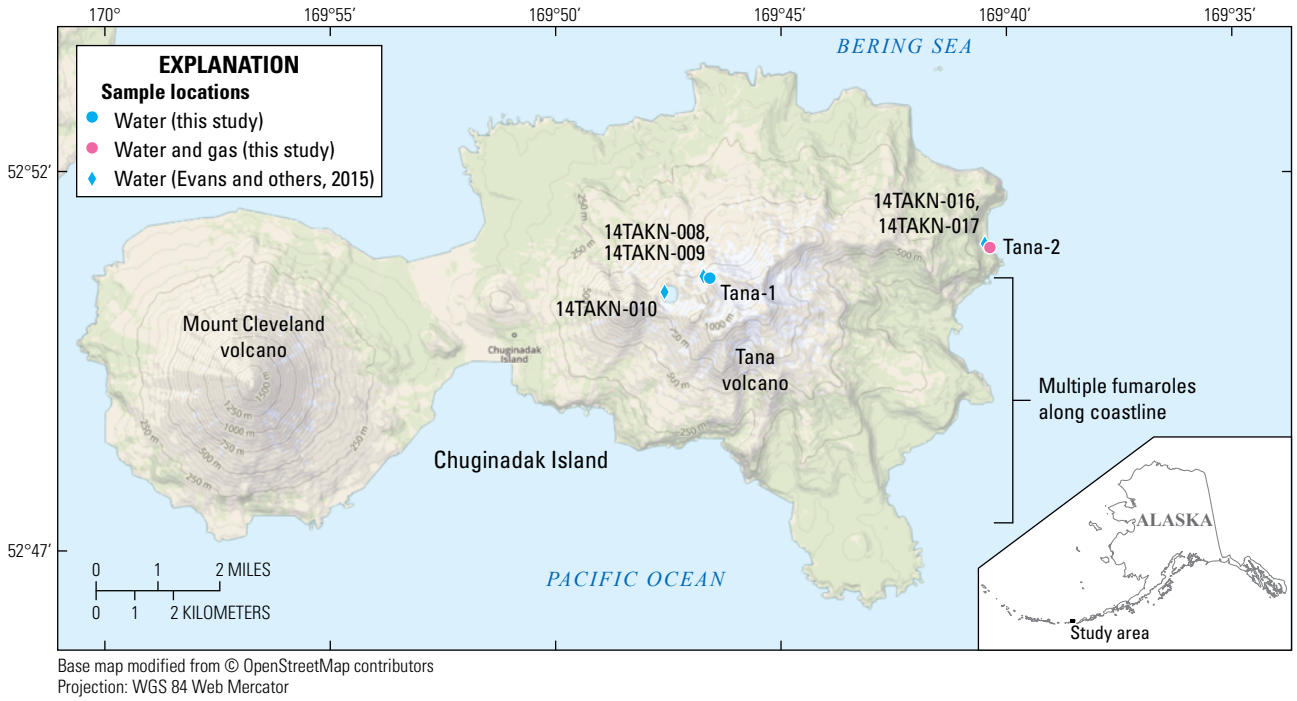

Figure 22. Map of Tana volcano east of Mount Cleveland on Chuginadak Island, August 2015 showing sampling locations from this study and from Evans and others (2015).

Figure 23. Photograph of the northern upper flank of Tana volcano, east of Mount Cleveland on Chuginadak Island (see Evans and others, 2015 for an overview photo of this area). The site contains multiple diffuse fumaroles and very low-flow springs in an approximately 400 meter-squared area. A picture of the water sample collected at Tana-1 is shown in figure 2. The MultiGAS instrument was placed several meters away from the fumarole. Temperature = 95 °C and pH = 6. U.S. Geological Survey photograph by Cynthia Werner.

Water Chemistry Summary

The δD and $\delta^{18}O$ values indicate a meteoric origin for all the springwaters from Tana volcano, which plot on or very near the meteoric water line (fig. 25). In terms of SO_4-HCO_3-Cl, Tana-1 is a steam-heated water, whereas Tana-2 plots between volcanic and mature geothermal waters (fig. 18). However, springwater chemical compositions show two separate trends with respect to Cl (fig. 26). The samples from the north flank are low in Cl and elevated in SiO_2, SO_4, Ca, and Mg (table 1). The high SO_4/Cl ratio likely indicates that the northern thermal area overlies a vapor-dominated system, where the high concentrations of cations result from rock dissolution from the acidic waters (Evans and others, 2015). This interpretation is consistent with the hydrothermal character of the gases emitted in this area (see below).

The waters from the east side of Tana volcano are elevated in Cl, bromide (Br^-), and sodium (Na), and are low in SiO_2 and other cations. The Cl/Br^- ratio of Tana-2 is 278, nearly identical to that of seawater (280) and supports the idea presented by Evans and others (2015) that the springs interact with seawater. Assuming the same sites were sampled in both years (we are fairly confident that we sampled in the same general location) the water chemistry varied with time. In 2014, SO_4 concentrations exceeded that of Cl, whereas in 2015, Cl exceeded SO_4. This change could indicate an increase in the seawater component relative to a steam-derived component during 2015.

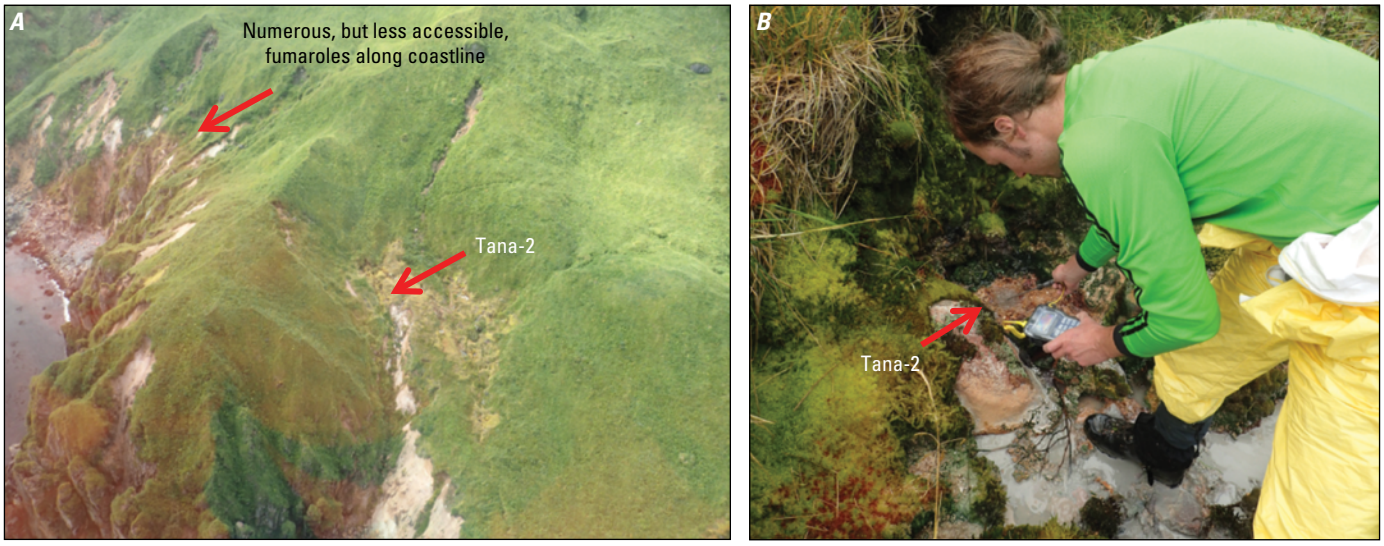

Figure 24. Photographs of the eastern coast of Tana volcano showing the location of the Tana-2 samples (*A*) and of Christoph Kern measuring the temperature of a small spring (*B*). Gas and water samples were collected at this location (T = 95.5 °C and pH = 3). U.S. Geological Survey photograph by Cynthia Werner.

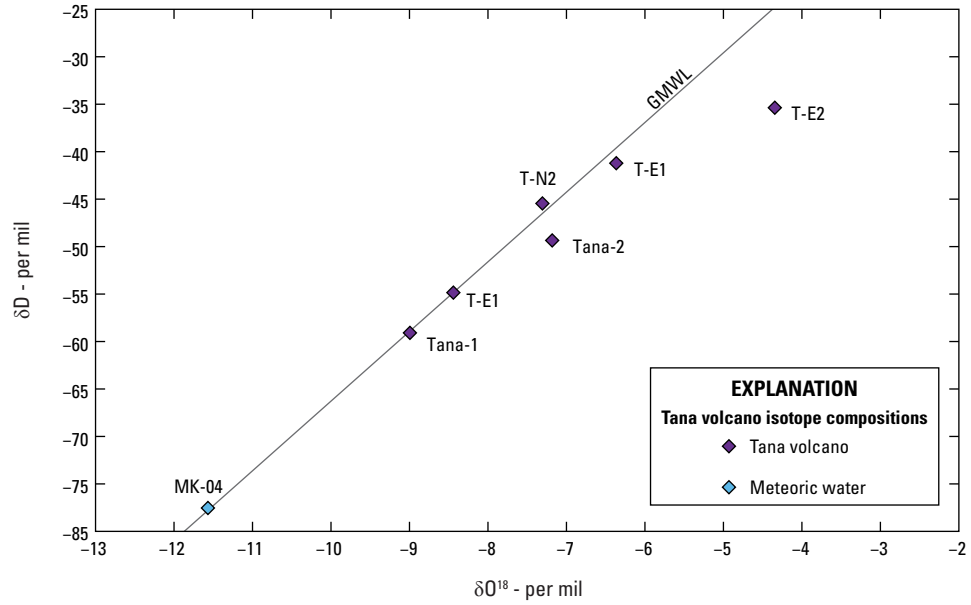

Figure 25. Stable Isotope plot of thermal waters in the north and east thermal areas at Tana volcano on Chuginadak Island from 2014 (T-N1, T-N2, T-E1, T-E2) and 2015 (Tana-1, Tana-2). MK-04 is a sample of meteoric water and plots on the Global Meteoric Water line (GMWL) shown in gray.

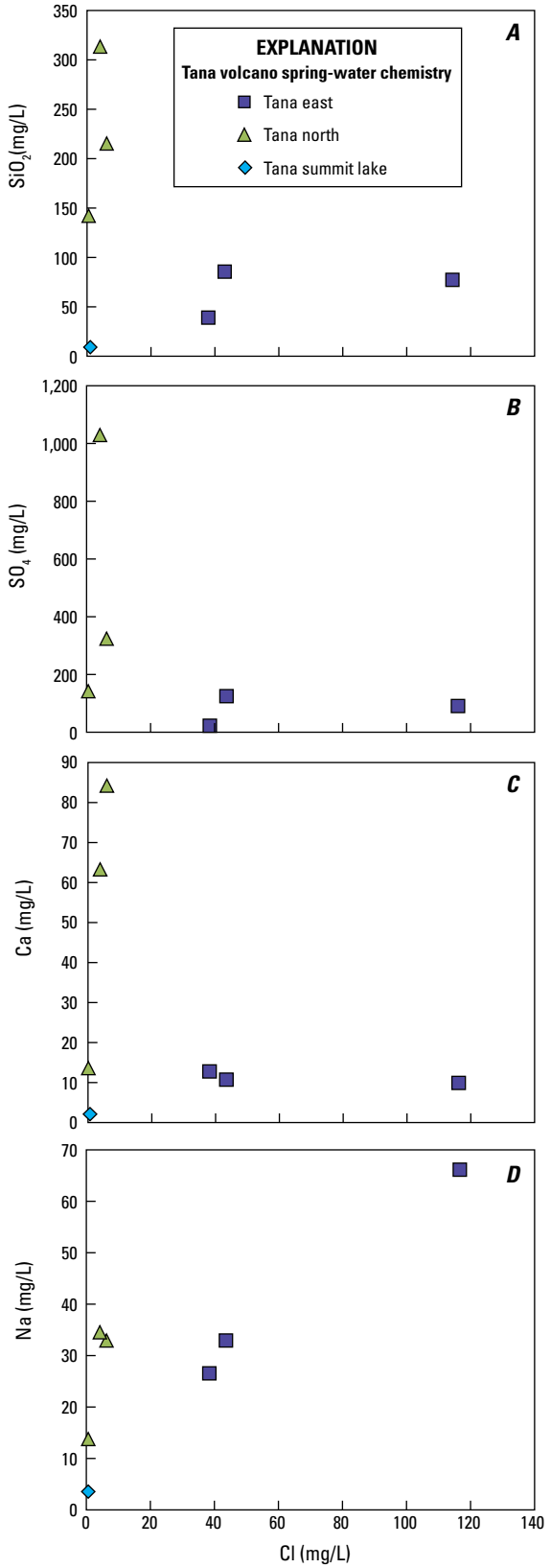

Figure 26. Scatterplots showing the constituent concentrations vs. chlorine (Cl) for thermal springwaters from Tana volcano in the east (purple square), north (green triangle), and summit crater lake (blue diamond) sampled in 2014 and 2015. Values are given in milligrams per liter (mg/L).

Gas Chemistry Summary

A gas sample was collected on the east side of Tana volcano (Tana-2; fig. 22), but MultiGAS data were collected at both locations. The gas from the bubbling spring on the east side of Tana volcano was enriched in CO_2 and H_2S with a CO_2/H_2S ratio of 76 (table 2). The MultiGAS CO_2/H_2S ratio was 93 at this site, where the difference most likely represents an enrichment in CO_2 due to diffuse gas sources around the instrument. In the north, the CO_2/H_2S ratio from the MultiGAS data was 23 (fig. 27), much lower than the ratio from sites in the east (fig. 28). Ratios in this range are consistent with a hydrothermal origin, and the lower value measured at Tana-1 location in the north is similar to that measured at hydrothermal areas at active volcanoes in the Cascades (Werner and others, 2009).

The relative abundances of N_2-He-Ar in gas collected on Tana volcano in 2015 plot along a mixing line between most of the 2015 Akutan Volcano gases and air (fig. 12). Like Makushin volcano, the Tana volcano gas plots off of the Cascade Range Aleutian Arc trend described by Symonds and others (2003) and instead plots approximately midway between magmatic and air endmembers.

Carbon and Helium Isotopes

Like the overall gas geochemistry, the carbon and helium isotopes for Tana-02 suggest the influence of magmatic gas. The $\delta^{13}C\text{-}CO_2$ value for Tana-2 (−9.65 per mil) is the second heaviest with respect to all samples collected in 2015, is similar to CO_2 from hot springs at the Emmons Lake Volcanic Center (−9.8 to −9.7 per mil; Evans and others, 2015), and is lighter than the range of typical isotopic values of carbon quoted for the upper mantle (for example, −5 to −8 per mil, Allard, 1983; Symonds and others, 2003). Likewise, the R_C/R_A value for helium from Tana-02 (6.43) is only slightly lower than other volcanoes in the Aleutian Islands that show a clear magmatic signature with little crustal contamination (for example, Mount Mageik, Trident volcano, and Mount Griggs all have values of 7.5 or higher).

Gas Geothermometry

Application of the D'Amore and Panichi (1980) gas geothermometer to the Tana volcano gas yields a temperature estimate of 215 °C, which is consistent with a hydrothermal origin. This is the first estimate of subsurface temperature available for this volcano.

Future Study Recommendations

Until 2014, there was no direct evidence of ongoing magmatic activity at Tana volcano, east of Mount Cleveland, which is one of the most active volcanoes in the Aleutian arc. In addition to the clear magmatic signature of the thermal features presented here, the morphology of Tana volcano and

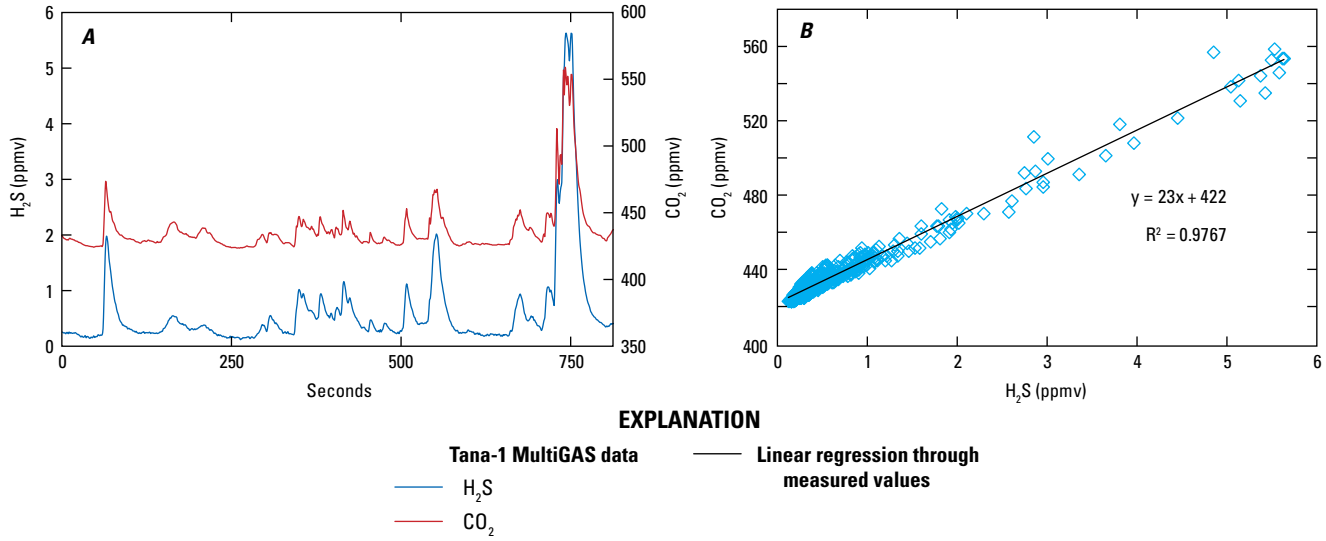

Figure 27. Graphs of CO_2 vs H_2S for the MultiGAS data collected near sample Tana-1 on August 12, 2015. *A*, Time series graph of the data with the peaks of CO_2 and H_2S corresponding in time (one sample per second). *B*, Graph displaying the regression of CO_2 to H_2S. Good correlation is observed between CO_2 and H_2S. CO_2/H_2S based on these data is approximately 23. Values are given in parts per million by volume (ppmv).

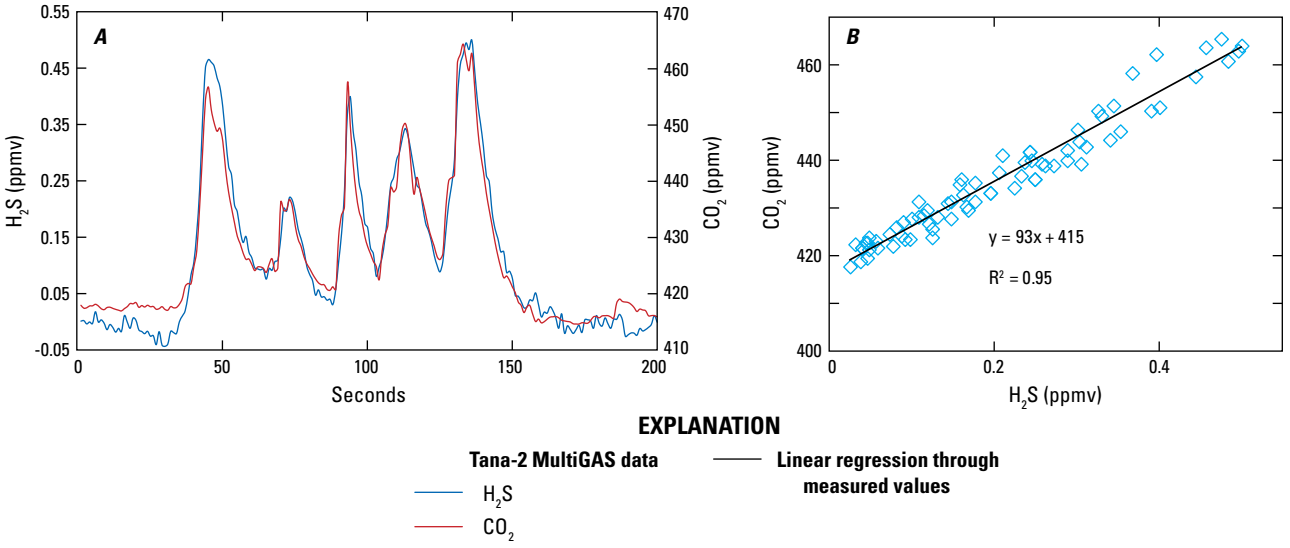

Figure 28. Graphs of CO_2 vs H_2S for the MultiGAS data collected near sample Tana-2 on August 14, 2015. A single-stage recursive filter was applied to the CO_2 data. *A*, Time series graph of the data with the peaks of CO_2 and H_2S corresponding in time (one sample per second). *B*, Graph displaying the regression of CO_2 to H_2S. Good correlation is observed between CO_2 and H_2S. CO_2/H_2S based on these data is approximately 93. Values are given in parts per million by volume (ppmv).

that of neighboring islands seems to provide ample evidence of recent volcanism (apart from that at Mount Cleveland). Thus, we would advise the continued investigation of all thermal features in the Islands of Four Mountains area, including the not-yet-sampled features noted in the crater of Herbert volcano. Future expeditions to Tana volcano should include gas and water samples from fumaroles and hot springs, paying particular attention to filling in gaps from this study and that of Evans and others, 2015 (for example, specifically obtaining a fumarolic gas sample at Tana-1 location) to monitor for changes in the geochemistry.

Extensive areas of fumarolic gas were noted along the eastern coastline of Chuginadak Island, and a second possible thermal area was observed on the north slope of Tana volcano that

was inaccessible (fig. 22). The use of a thermal infrared camera from an airborne platform might provide information on the extent and location of other thermal features on the island, although with the abundant sunlight in the summer months it might be difficult to detect small anomalies. Flights of this type should occur in the early morning hours.

Fisher Caldera

Fisher Caldera is a large volcanic complex located on Unimak Island between Shishaldin and Westdahl volcanoes (fig. 29), both of which have experienced historical eruptions. Fisher Caldera hosts the largest of 12 Holocene calderas in Alaska and is located at the center of the most active part of the Aleutian arc, which experiences the highest rate of convergence (Stelling and others, 2005). The caldera-forming eruption has been dated at 9100 years before present (YBP), and the most recent post-caldera eruptions have been from Turquoise cone, an informally named volcanic vent on the southern margin of Fisher Caldera. The last eruption was from mount Finch, an informally named topographic feature in Fisher Caldera, in 1826 and was andesitic/dacitic in composition (fig. 30). There are several sites of active degassing and thermal activity in Fisher Caldera, and to our knowledge these are the first samples collected at these locations.

Fisher Caldera has been the focus of several geophysical studies that indicate the caldera is subsiding over decadal timeframes. InSAR data that spanned from 1992 to 2000 showed the central part of the caldera subsided about 1.5 cm/year during that period (Lu and Dzurisin, 2014). Lu and Dzurisin (2015) fit the observed subsidence pattern equally well with a Mogi-type source, a sill-like source, and a spheroidal source, each located near the center of the caldera and in the depth range 3.5–8.5 km below sea level. Gong and others (2015) also measured ongoing subsidence by GPS between 2008 and 2011, and they identified similar source parameters for a deflating sill centered beneath the caldera. Subsidence was thought to occur because of either degassing and thermal contraction of a crystallizing magma body or depressurization of the hydrothermal system (Mann and Freymueller, 2003; Lu and Dzurisin, 2015, Gong and others,

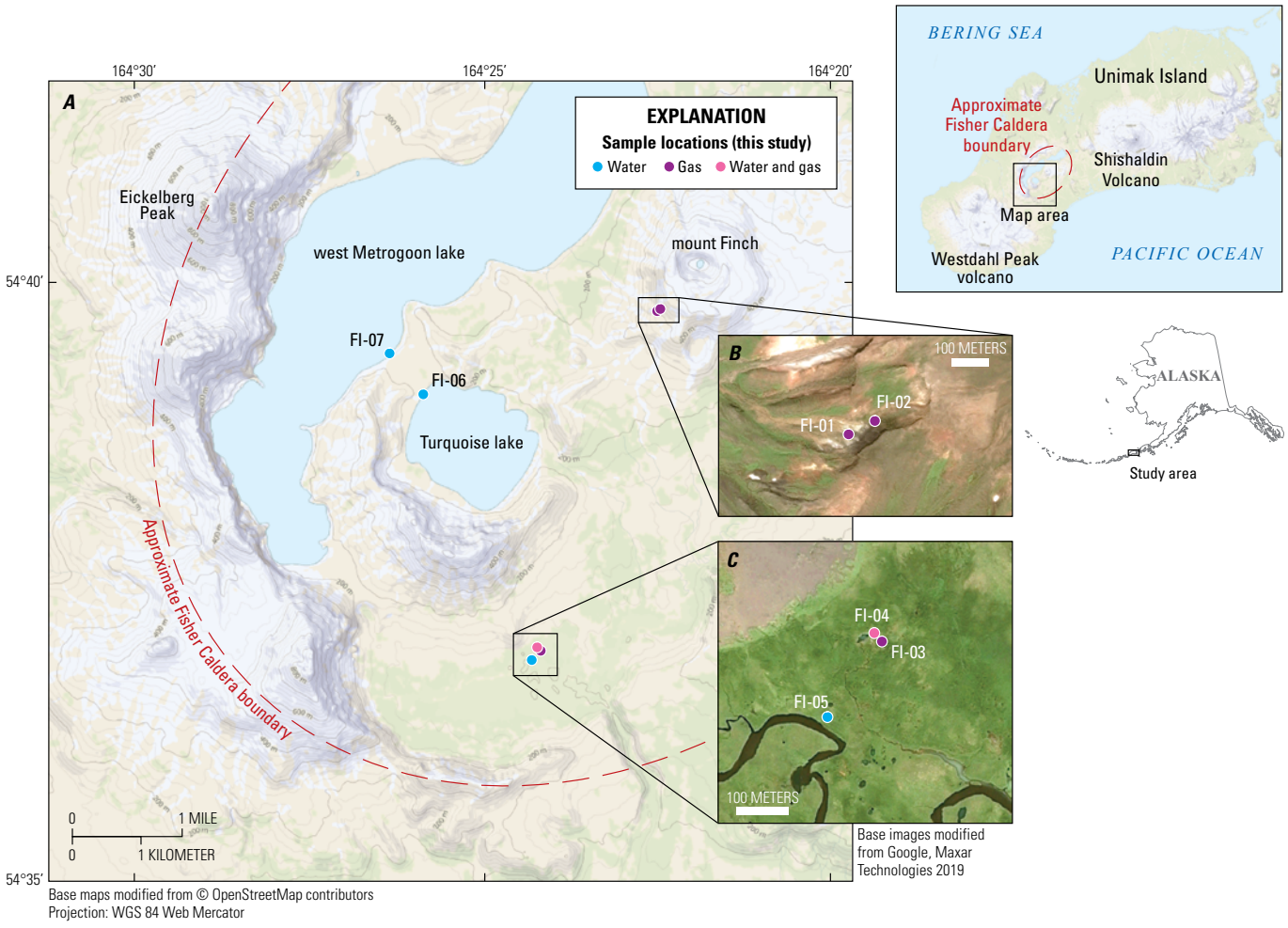

Figure 29. Map (*A*) and satellite images (*B* and *C*) showing sampling area between Westdahl Peak volcano and Shishaldin Volcano on Unimak Island. Both 29*A* and the location map show the approximate location of the Fisher Caldera (red dashed line), and water and (or) gas sample locations are shown on 29*A*, 29*B*, and 29*C*.

2015). Lu and Dzurisin (2015) suggested that future seismic and geodetic observations might help to distinguish between the two mechanisms proposed by Mann and Freymueller (2003) to explain the long-term subsidence.

There have been no geochemical studies of gas and waters from Fisher Caldera, but satellite images of the lake next to Turquoise cone show evidence of degassing manifestations in the lake that could be the result of hydrothermal activity in the past. A circular feature is sometimes observed in air photos of the lake that could be related to the upwelling of gases, and the lake changes from green to aqua blue from image to image, which is also likely related to changes in degassing. In addition, multiple areas of acid alteration exist in the interior of the caldera, some of which host weak fumarolic activity (Stelling and others, 2005). In 2015, three areas, located at Mount Finch, the intra-caldera lakes, and the warm springs in the southern part of the caldera, were targeted for sampling (fig. 30).

Mount Finch and Caldera Sampling

Mount Finch is located in the center of Fisher Caldera and is the site of the most recent volcanism and locus of the observed subsidence (fig. 29*B*). Mount Finch hosts at least one area of active degassing on the lower north flank of the cone (figs. 31 and 32), although multiple altered areas are located on mount Finch as viewed in satellite images. We sampled an approximately 75×150-meter (m) area that hosted multiple boiling-temperature fumaroles and steam-heated ground (fig. 31).

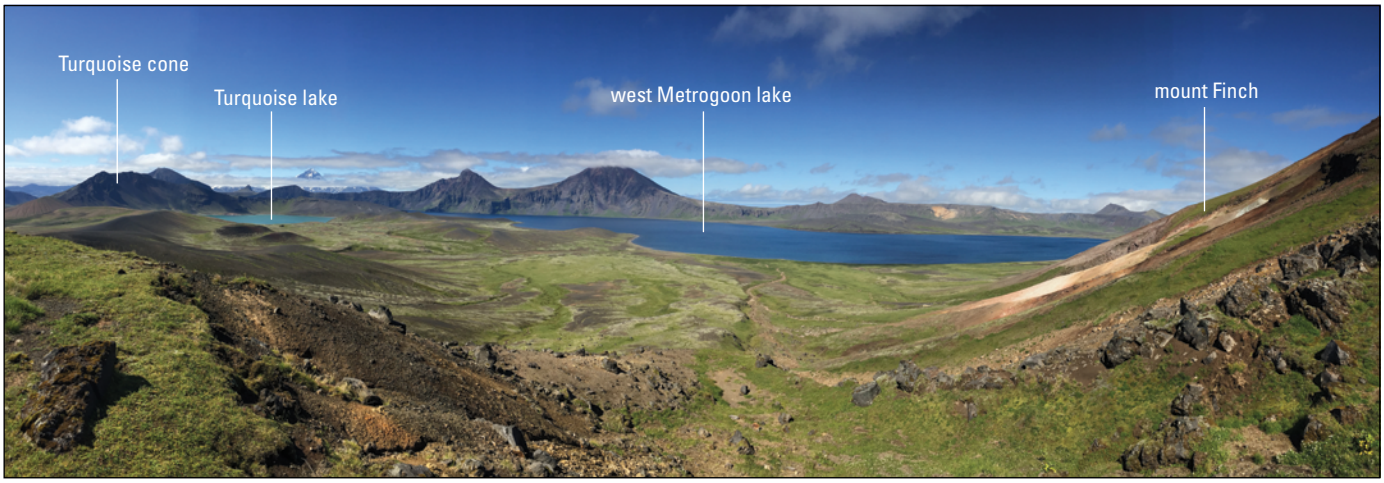

Figure 30. Panoramic photograph viewing the northern interior of Fisher Caldera from a ridge near mount Finch, an informally named feature near the central area of Fisher Caldera. The panorama spans a region of at least 6 km, within the caldera that is 16 km in length and 11 km in width. Samples were collected at the informally named Turquoise lake, west Metrogoon lake, and mount Finch. U.S. Geological Survey photograph by Cynthia Werner.

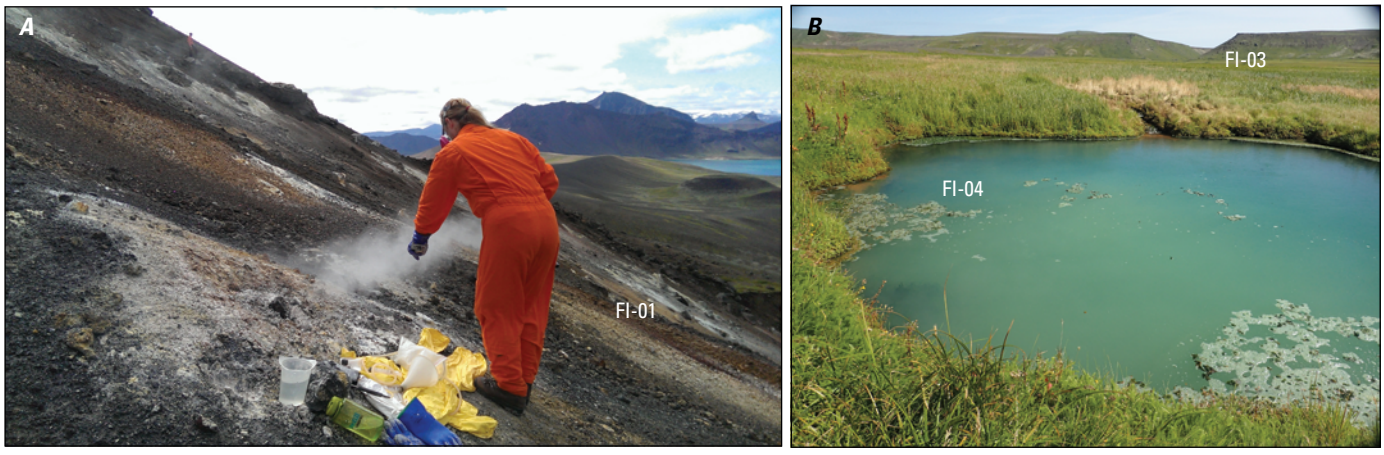

Figure 31. Photographs of area sampled on mount Finch, an informally named volcanic cone near the central area of Fisher Caldera. *A*, Photograph looking southwest of Cynthia Werner measuring temperature of gas vent. MultiGAS instrument placement shown near FI-01 in figure 4. *B*, Photograph of the caldera warm springs sample locations FI-04 and FI-03. U.S. Geological Survey photographs by Christoph Kern and Cynthia Werner.

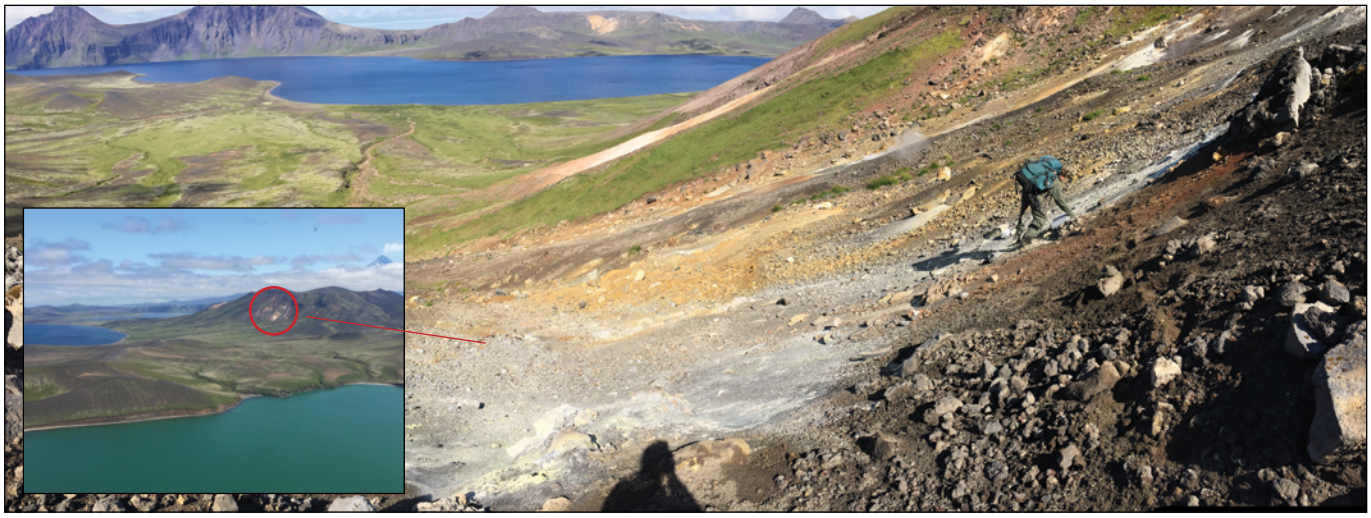

Figure 32. Photographs looking northeast of the area sampled on mount Finch, an informally named volcanic cone near the central area of Fisher Caldera. Christoph Kern navigates across the steep terrain to access the area of degassing vents. The inset photograph shows the location of the sampling area on the base of the north flank of mount Finch. U.S. Geological Survey photographs by Cynthia Werner.

In the caldera, we sampled two of the three large caldera lakes (west Metrogoon lake, an informally named lake on the western margin of Fisher Caldera and Turquoise lake, an informally named lake that is often turquoise and is in southwestern Fisher Caldera) (figs. 29 and 31). Of the two, Turquoise lake had the lowest pH (1.7) (table 1). Water samples were also collected in the southeastern part of the caldera, which hosts a boggy area with several warm springs that issue through alluvium. The springs were difficult to locate on foot, and thus only a few samples were taken. More springs likely exist based on closer inspection of Google Earth images of the caldera area.

Water Chemistry Summary

The δD and $\delta^{18}O$ values for all water samples from Fisher Caldera plot near to the meteoric water line (fig. 33) and indicate a meteoric origin. The springs and Turquoise lake samples are all elevated in SiO_2 and SO_4, indicating modification due to hydrothermal processes (fig. 34).

In regard to geothermal prospecting, the waters we sampled from the caldera-floor springs are 'immature', which means they are not in equilibrium with the underlying reservoir rocks. The high SiO_2 content reflects disequilibrium between rapid release from the dissolving aquifer minerals and slow precipitation of quartz or chalcedony, so SiO_2 correlates well with Mg, Na, and Ca. The reservoir temperature is lower than the quartz or chalcedony geothermometers (plot not shown), which indicates a temperature of 155–177 °C. This suggests the reservoir temperature might not be much higher than the discharge temperature. All of the waters sampled in Fisher Caldera, except for Turquoise lake (FI-06), plot in the peripheral section of the SO_4-Cl-HCO_3 ternary diagram (fig. 18), which means they have elevated HCO_3 relative to SO_4 or Cl and likely lie further along the outflow path from the hydrothermal source region where HCO_3 increases with time and distance. The waters from Turquoise lake have a pH of 1.73, and therefore have no HCO_3, and plot in the volcanic waters section of the ternary diagram (fig. 18). The elevated SO_4 in the lake waters that drives the low pH supports the hypothesis that a considerable amount of magmatic degassing must acidify the lake given the relatively large lake volume.

Examination of springwater Cl concentrations plotted versus other major components indicates the Fisher Caldera waters share a common source (fig. 34). The two hot springs sampled in Fisher Caldera (FI-03 at 48.3 °C and FI-04 at 46 °C) have similar chemistry, although Fl-03 is slightly more concentrated in Cl than FI-04 (table 1). The stream that drains to the south through the caldera floor (sample FI-05) seems to be springwater diluted by water similar to west Metrogoon lake. The lake sample (FI-07) was the most dilute sample collected and plots near 0 for all measured analytes on figure 34. For some analytes Turquoise lake (FI-06) also plots on the same dilution trend and is the most concentrated water in terms of SO_4, Cl, K, and Li. For many other analytes though, Turquoise lake appears as a distinct water with a separate source. The stable isotope composition of all of the water samples plot off of the GMWL (fig. 33), which is likely due to evaporation in the case of the crater lakes and the pool-type warm springs.

The springwaters share a common source that is rich in HCO_3, SO_4, and Mg, and moderately high in Ca and SiO_2. The chemistry of the springs may reflect the reaction of magmatic CO_2 and groundwater, which dissolves aquifer minerals as conversion to HCO_3 occurs and elevates cation concentrations. Unreacted CO_2 would show up in the gas bubbles.

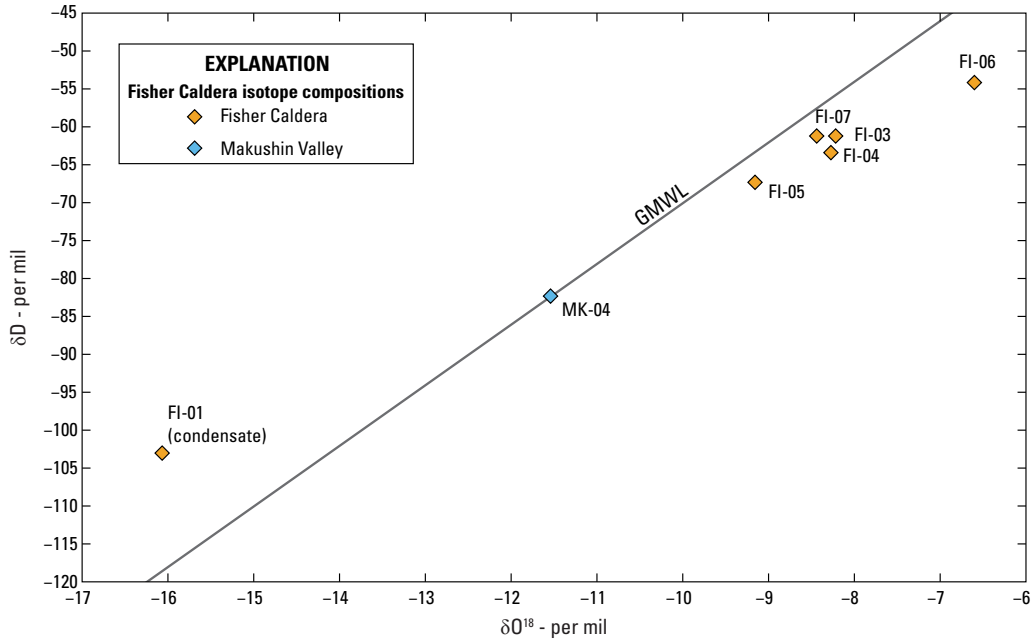

Figure 33. Stable isotope composition of thermal waters from Fisher Caldera. Sample MK-04 is a meteoric water from Makushin Volcano and is plotted to show the meteoric water trend in the region. Spring (FI-03 and FI-04) and crater lake waters (Turquoise lake, FI-06, and west Metrogoon lake, FI-07) are shifted to the right of the Global Meteoric Water Line (GMWL) likely because of evaporation. The stream sample from Fisher Caldera (FI-05) also is shifted slightly to the right of the GMWL. The fumarole steam condensate from mount Finch (FI-01) plots far to the left of the GMWL because of isotope fractionation during boiling and separation of the steam.

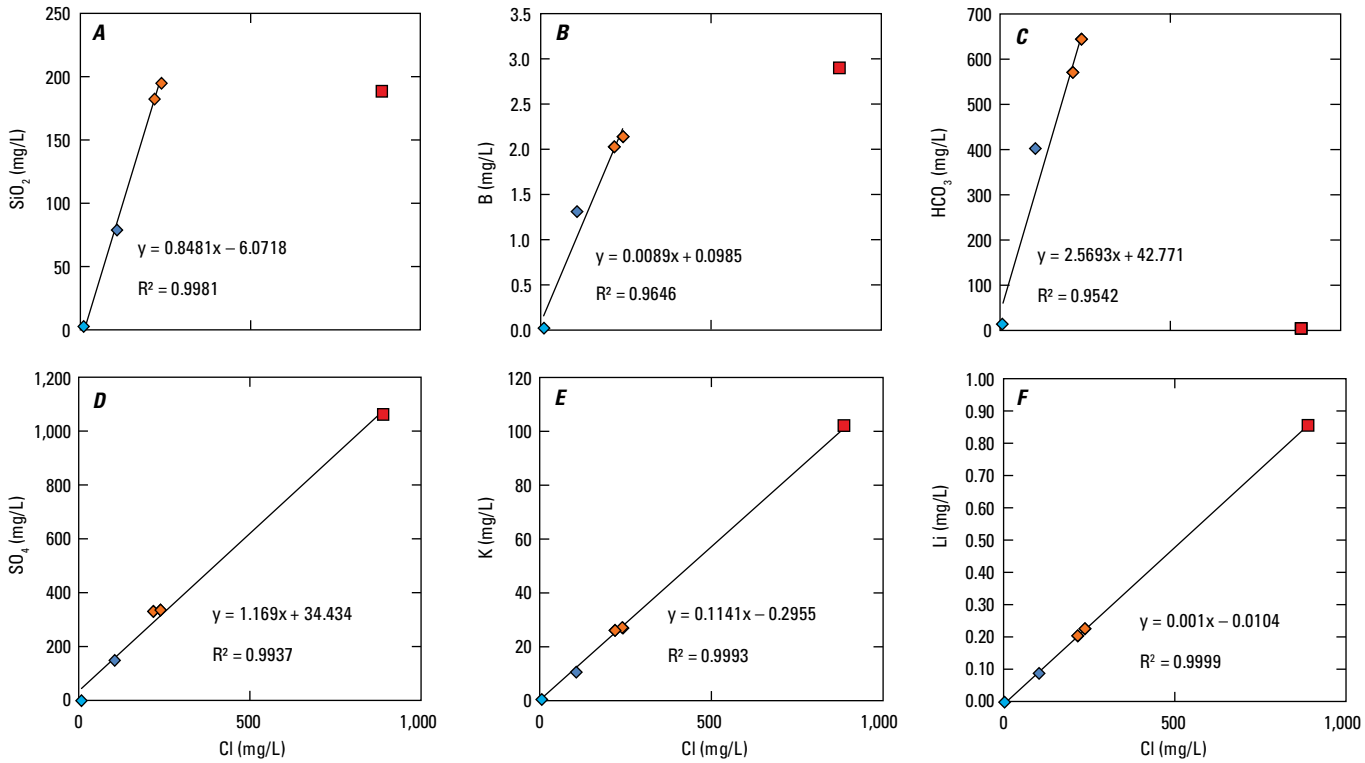

Figure 34. Selected chemical plots for the waters sampled from Fisher Caldera on August 19, 2015. Chlorine (Cl) concentrations in the warm springs collected on the southern caldera floor (FI-03 and FI-04) and stream samples (FI-05) are well correlated with major and trace components. Cl concentrations in Turquoise lake (sample FI-06) correlate with some components, but SiO_2, boron (B) and HCO_3 concentrations fall off the hot spring-creek water trend. West Metrogoon lake was dilute and not plotted. Values are given in milligrams per liter (mg/L).

Gas Chemistry Summary

The gas samples taken on mount Finch are hydrothermal in character, however they differ from the gases from the other hydrothermal areas in the Aleutian Islands sampled in 2015. Specifically, the high H_2 and H_2S concentrations in addition to the low CH_4 concentrations are all indicative of a high-temperature source for the gases from mount Finch. These properties indicate, but do not demonstrate, the presence of magma at shallow depths. Lack of CO or SO_2 (<0.005%) suggest that one or more hydrothermal systems overlies the magma and scrubs these gases out. The lack of superheated conditions, plus the isotopes of condensed steam, suggest that mixing and boiling of a shallow groundwater system is involved as well. The data are reasonably consistent with the geodetically derived hypothesis about the cooling sill at depth, but the gases are also influenced by changes within a hydrothermal system. The N_2-He-Ar ternary diagram is not useful for the Fisher Caldera gas samples because He concentrations were below detection limits.

The CO_2/H_2S ratios for the two fumarole gases (samples FI-01 and FI-02) were approximately 15, whereas the MultiGAS value ranged between 18–21 (table 2; fig. 35). The slightly higher values in the MultiGAS data likely result from the unit being placed in an area of diffuse CO_2 emission with lesser amounts of H_2S, similar to that observed in other hydrothermal areas in this study.

Carbon and Helium Isotopes

As with the overall gas geochemistry, the carbon and helium isotopes for FI-01 demonstrate the influence of a magmatic component. The $\delta^{13}C$–CO_2 value for FI-01 (−7.32 per mil) is the heaviest with respect to all samples collected in 2015 and is indistinguishable from values characteristic of the upper mantle (−5 to −8 per mil, Allard, 1983; Symonds and others, 2003). Likewise, the R_C/R_A value for FI-01 (8.08) is the highest He isotope ratio from our sample suite and represents one of the most mantle-like samples in Alaska with little crustal contamination (for example, Mount Mageik, Trident Volcano, and Mount Griggs all have values of 7.5 or higher).

Gas Geothermometry

The reservoir temperature estimate for the fumaroles was 390 °C using the D'Amore and Panichi (1980) geothermometer and the highest of all the sites visited in 2015. However, the calculated temperature is outside of the calibrated range for this geothermometer, so the values may not be accurate. If we, as an example, assume a redox potential $R_H = X_H/X_{H2O} = -3.21$ (suggested for Yellowstone by Chiodini and others, 2012), and plot the fumarole compositions on log (H_2/H_2O) vs. log (CH_4/CO_2), they plot near the point for 350 °C vapor, thus providing confidence in the high geothermometer-derived temperature. That such a high-temperature reservoir may exist beneath mount Finch is consistent with cooling of a shallow intrusion. However, given that it has been nearly 200 years since there was a magmatic eruption at mount Finch, the geothermometer results and the carbon and helium isotope data support continued input or connectivity with a deeper and still-active magmatic system fed ultimately by mantle-derived basalt.

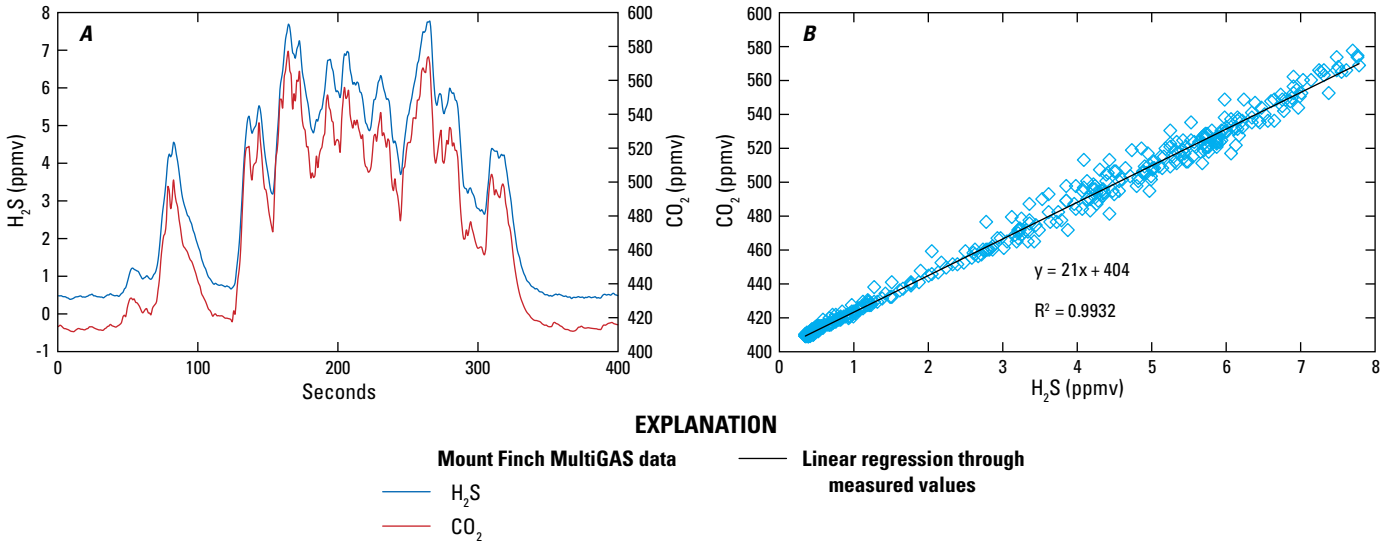

Figure 35. Graphs of MultiGAS data collected near sample FI-01 on mount Finch, an informally named volcanic cone near the central area of Fisher Caldera, on August 19, 2015. *A*, Time series graph of the data with the peaks of CO_2 and H_2S corresponding in time (one sample per second). *B*, Graph displaying the regression of CO_2 to H_2S. Good correlation is observed between CO_2 and H_2S. CO_2/H_2S based on these data is approximately 21. Values are given in parts per million by volume (ppmv).

Future Study Recommendations

Future studies concerning volcano hazards monitoring at Fisher Caldera should focus on mount Finch and Turquoise lake as these areas are the most recently active vents in the area and show the strongest magmatic signature. More work could be done to assess the nature of upwelling in Turquoise lake and the chemistry of water from this zone, perhaps even collecting a depth profile in the lake. Review of satellite time series data may be able to determine the timing of upwelling episodes that may be related to the periodic release from a subsurface magmatic or hydrothermal system. Observations of active degassing from the lake should also be documented if field parties visit the area again.

Geyser Bight Hydrothermal Area

The Geyser Bight hydrothermal area is located on Umnak Island in the Aleutian arc between the Okmok Caldera and Mount Recheshnoi volcanoes (fig. 36). According to Motyka and others (1993), Geyser Bight is one of the hottest and most extensive areas of thermal activity in Alaska outside the active volcanic vents. The heat driving hydrothermal activity in the region is associated with magmatic intrusions at Recheshnoi volcano (Motyka and others, 1993), the summit of which lies approximately 10 km to the southwest. Recheshnoi volcano has had no historical eruptions but is thought to have been active in the Holocene. The area was visited twice in the 1980s as part of a study to assess geothermal potential in the area, and it was not visited again until this study as far as the authors are aware. The Geyser Bight area was visited again during a 2016 field campaign.

Evidence that a magmatic heat source drives thermal activity came from analyses of volcanic fumaroles (Nye and others,1992), which showed a clear magmatic signature in helium isotopes ($R_C/R_A = 7.4$). The conservative estimate of thermal output in 1988 was 16.7 megawatts, during which time hot spring discharge was estimated at approximately 3,250 liters per minute. This estimate is lower than the 1946 estimate of 4,150 liters per minute. The decline of outflow was suggested to be caused by silica deposition along upflow paths between 1948 and 1988 (Motyka and others, 1993).

Fumaroles, hot springs, and alteration are extensive in several thermal areas that cover approximately 4 square kilometers, as estimated by Nye and others (1992). Thorough sampling of this area would require around a week of time. We had less than a full day, in which we were able to sample features in three of the six thermal areas identified by Nye and others (1992) and Motyka and others (1993). These samples were sourced from the two uppermost fumarole fields ("F1" and "F2" of Nye and others (1992), fig. 37), and the "G" hydrothermal area along Geyser Creek (fig. 38).

All of the thermal areas were mapped in detail by Nye and others (1992), and the comparison of thermal water compositions in 2015 with those of Motyka and others (1992) suggests that the water chemistry did not change considerably over the 30–40 years between sampling (fig. 39).

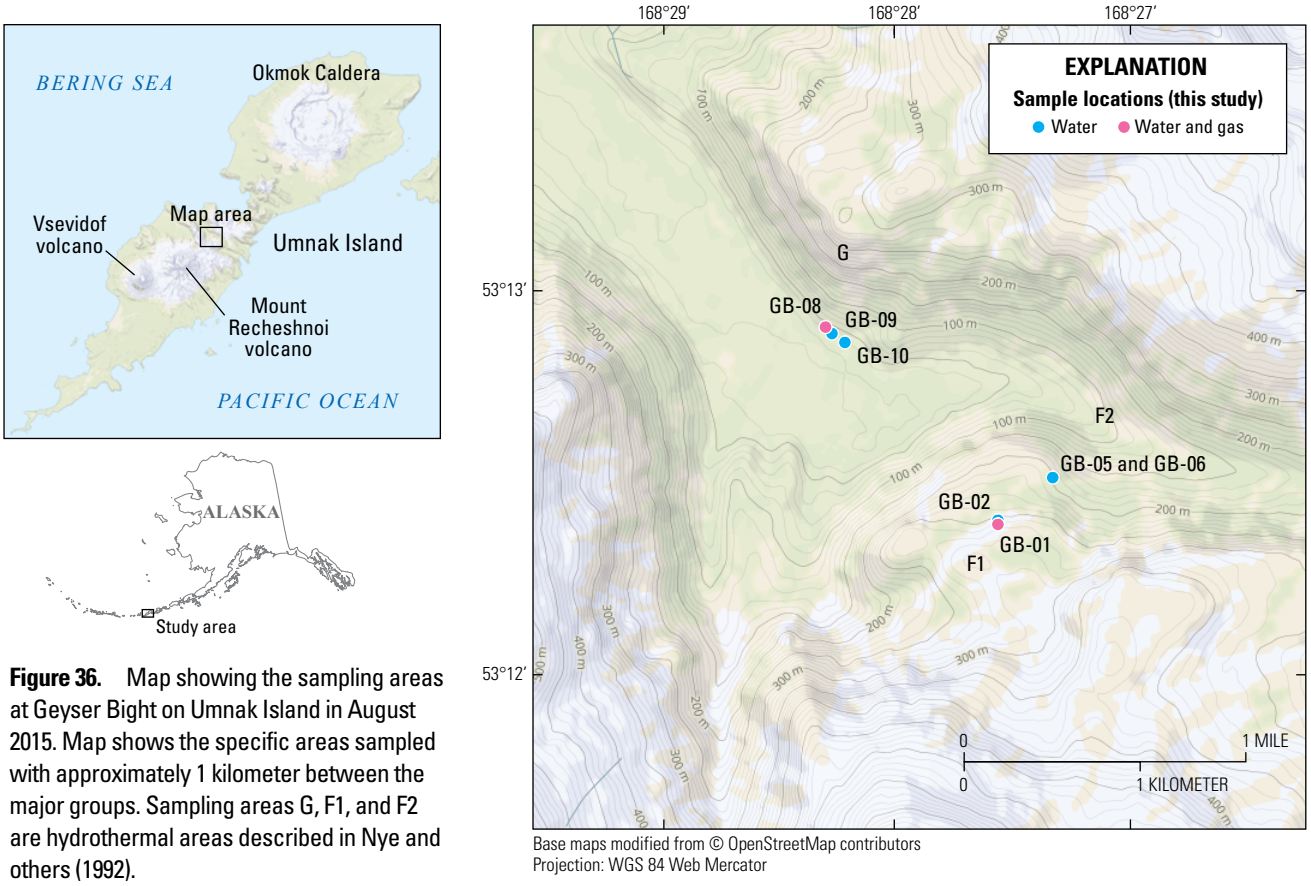

Figure 36. Map showing the sampling areas at Geyser Bight on Umnak Island in August 2015. Map shows the specific areas sampled with approximately 1 kilometer between the major groups. Sampling areas G, F1, and F2 are hydrothermal areas described in Nye and others (1992).

Figure 37. Photographs of the uppermost fumarole area (F1 area of Nye and others, 1992) in Geyser Bight (Christoph Kern for scale). *A*, The circled feature is GB-01 (fumarole). This area alone likely hosted several 10s of gas vents. *B*, Image of site GB-02 in the F1 thermal area. The feature had low discharge (< 1 liter per second). Temperature = 47 °C and pH = 3. U.S. Geological Survey photographs by Cynthia Werner.

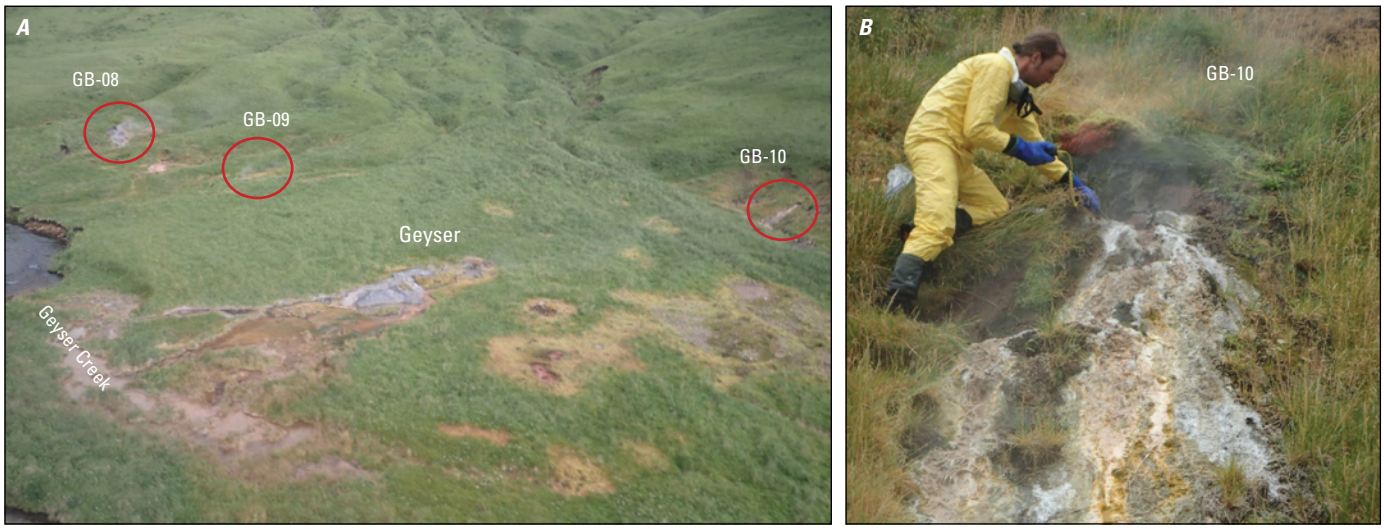

Figure 38. Photographs of the "G" hydrothermal area of Nye and others (1992) on Umnak Island. *A*, Photograph looking north along Geyser Creek that is flowing to the northwest. Sample locations are shown; the geyser was not sampled. *B*, Photograph of Christoph Kern measuring the temperature at the location of sample GB-10, the sample found to have the least amount of dilution by shallow groundwater (see text for further discussion). U.S. Geological Survey photographs by Cynthia Werner.

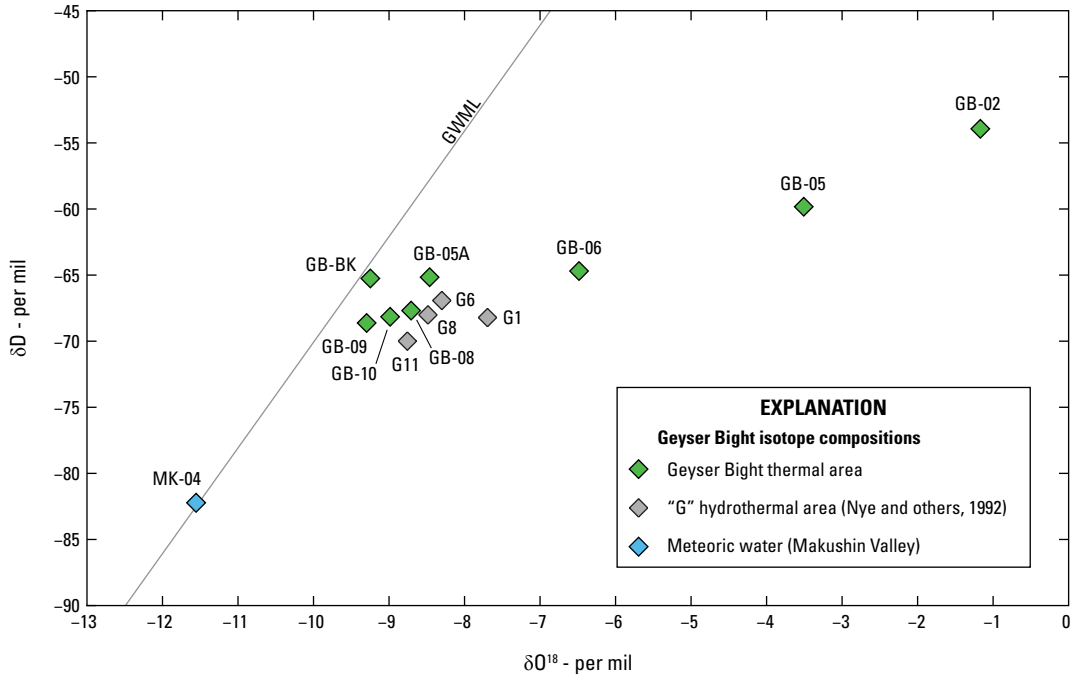

Figure 39. Graph showing stable isotope data for waters from the Geyser Bight thermal area collected in 2015 (green) and from the "G" hydrothermal area (in gray) of Nye and others (1992). GB-06, -05, and -02 are from low discharge springs in the fumarole areas F1 and F2 and show the largest deviation from the Global Meteoric Water Line (GMWL). The "G" hydrothermal area samples (for example, GB-09) from 2015 plot in close proximity to those from the same area sampled in 1988 and slightly shifted to the right of the GMWL. Meteoric waters (GB-BK and MK-04 from Makushin Valley) plot on or very near the GMWL.

Water Chemistry Summary

The isotope composition of all of the thermal water samples collected in Geyser Bight plot to the right of the GMWL (fig. 40). GB-BK is a background sample collected in a small lake upstream of the F1 fumarole field and plots very near the global meteoric water line (figs. 36 and 40). The 2015 samples from the "G" hydrothermal area cluster with those sampled from 1988, and the samples from fumarole fields F1 and F2 lie considerably further to the right of the GMWL. Motyka and others (1993) attributed the isotopic shift to dilution and boiling. We attribute the greater shift in the F1 and F2 samples to evaporation because these acidic features had minimal flow relative to the surface area of the spring.

The water chemistry of the springs sampled in 2015 is very similar to that of springwaters from the 1980s reported by Nye and others (1992) and Motyka and others (1993) (fig. 39). In terms of SO_4-HCO_3-Cl, the Geyser Bight samples from the "G" hydrothermal area are slightly less mature than those sampled at Akutan Volcano and are nearly identical to the samples collected in the 1980s in this area (fig. 18). The spring samples from the F1 and F2 areas (GB-02, -05, and -06) plot in the steam-heated region of the ternary diagram showing the relative abundance of SO_4 relative to Cl and HCO_3. This, combined with the near absence of Cl in these waters, demonstrates that little to no hydrothermal parent water is issuing in this area. Rather, the springs represent the condensation of steam in the shallow meteoric water, where the high SO_4 is the result of oxidation of H_2S, resulting in acidic and low-flow features. Typically, such fluids are observed in the upflow area of the hydrothermal system where the steam separates from the boiling water.

The 2015 samples from the "G" hydrothermal area plot on the same compositional trends as those collected during the 1980s (Motyka and others, 1993) (fig. 39). These trends represent dilution of parent geothermal waters with shallow meteoric waters. The trend is most striking for Na vs. Cl and boron (B) vs. Cl (fig. 39) and demonstrates that the waters are all related to a deep hydrothermal aquifer (Motyka and others, 1993).

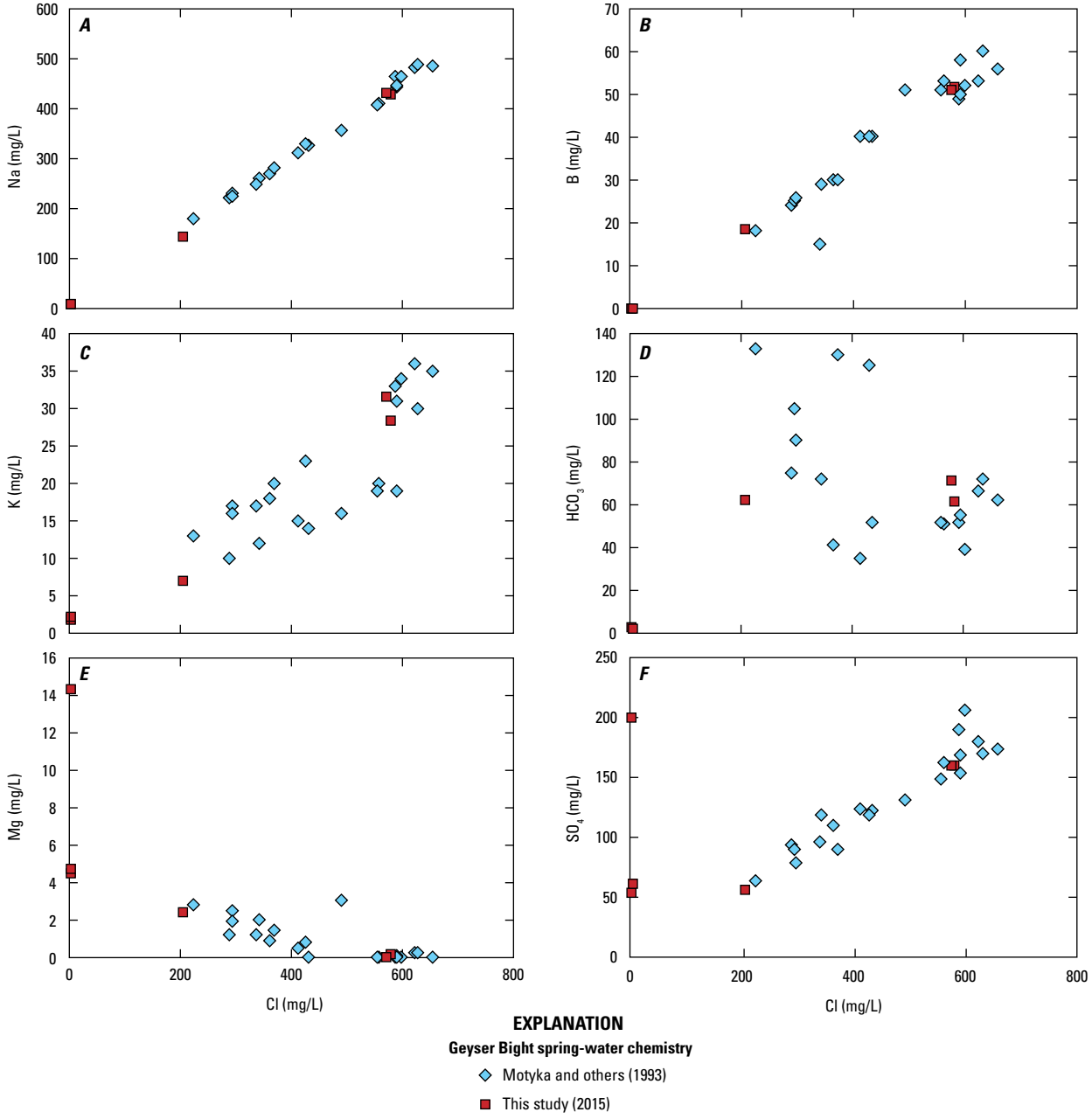

Figure 40. Graphs displaying constituent concentrations vs. chlorine (Cl) for thermal springwaters from the 1980s (blue diamonds, Nye and others, 1992; Motyka and others, 1993) and 2015 (red squares) given in milligrams per liter (mg/L). The 2015 springs sampled from the "G" area as defined by Nye and others (1992) is largely consistent with those in the 1980s, plotting amongst the previously analyzed data. Springs sampled in 2015 from the "F1" and "F2" areas defined by Nye and others (1992), however, plot along the y-axis showing little measurable chloride.

It is not common for high temperature hydrothermal waters to have appreciable Mg due to hydrothermal reactions, and the lack of Mg in the waters that contain > 500 milligrams/liter Cl suggests that those springs are the most pristine of those sampled. The inverse correlation observed between Cl and Mg (fig. 39) suggests that the ascending waters are diluted by lower temperature springwaters, as also suggested by Motyka and others (1993). Our samples from the fumarolic areas "F2" and "F1" as defined by Nye and others (1992) plot as a continuation of the dilution trend noted in Motyka and others (1993). Sample GB-02 (from the "F1" area) shows higher Mg than GB-05 and GB-06 from the "F2" area (fig. 39), which likely results from the dissolution of rock by the acidic water.

As noted by Motyka and others (1993), the Geyser Bight samples from the "G" hydrothermal area have very high arsenic (As) and barium (B) concentrations. High arsenic is thought to be the result of leaching of rocks, and the nearby rhyolites have very high concentrations of As compared to rhyolites elsewhere (table 1). Elevated B could result from interaction with sedimentary rock units that outcrop elsewhere in the region and may underlie the hydrothermal areas of Geyser Bight (Motyka and others, 1993). Alternatively, Motyka and others (1993) suggest that the elevated B could result from degassing of the magma in the subsurface.

Fluid Geothermometry

Water samples from Geyser Bight, like Akutan Volcano, provide data that are suitable for the use of fluid geothermometers (fig. 18). The data suggest that some waters are at equilibrium and other waters show trends approaching equilibrium. Both the quartz and the Na-K-Mg geothermometers (fig. 18) suggest equilibrium temperatures of approximately 200–210 °C. Nearly identical results were found for the "G" hydrothermal area samples presented in Motyka and others (1993). Through more extensive sampling and application of the SO_4-H_2O oxygen isotope geothermometer, Motyka and others (1993) suggest that two hydrothermal reservoirs exist for the Geyser Bight area, the hottest with a temperature of 265 °C.

Gas Chemistry Summary

The Geyser Bight gas samples had low gas to steam ratios and were contaminated by air either during sampling or sometime thereafter. A 2016 gas sample collected over steaming ground (T = 100 °C) approximately 200 m southeast of G-08 had a similarly low gas to steam ratio, with high contributions of atmospheric air (Deb Bergfeld, personal communication, May 2017). After correction for steam and air, the gas contains mostly CO_2 and H_2S, and the ratio of the corrected values suggests a CO_2/H_2S of 52. This is slightly higher than what was observed by MultiGAS, where a CO_2/H_2S of 45 was calculated (fig. 41). This is the opposite trend compared to other sites where the MultiGAS data showed higher CO_2/H_2S presumed to be due to it being placed in areas of high diffuse degassing of CO_2. Considering the air contamination of the direct gas sample, these values are consistent with one another and represent a typical hydrothermal composition. MultiGAS data collected in the "G" hydrothermal area along Geyser Creek had

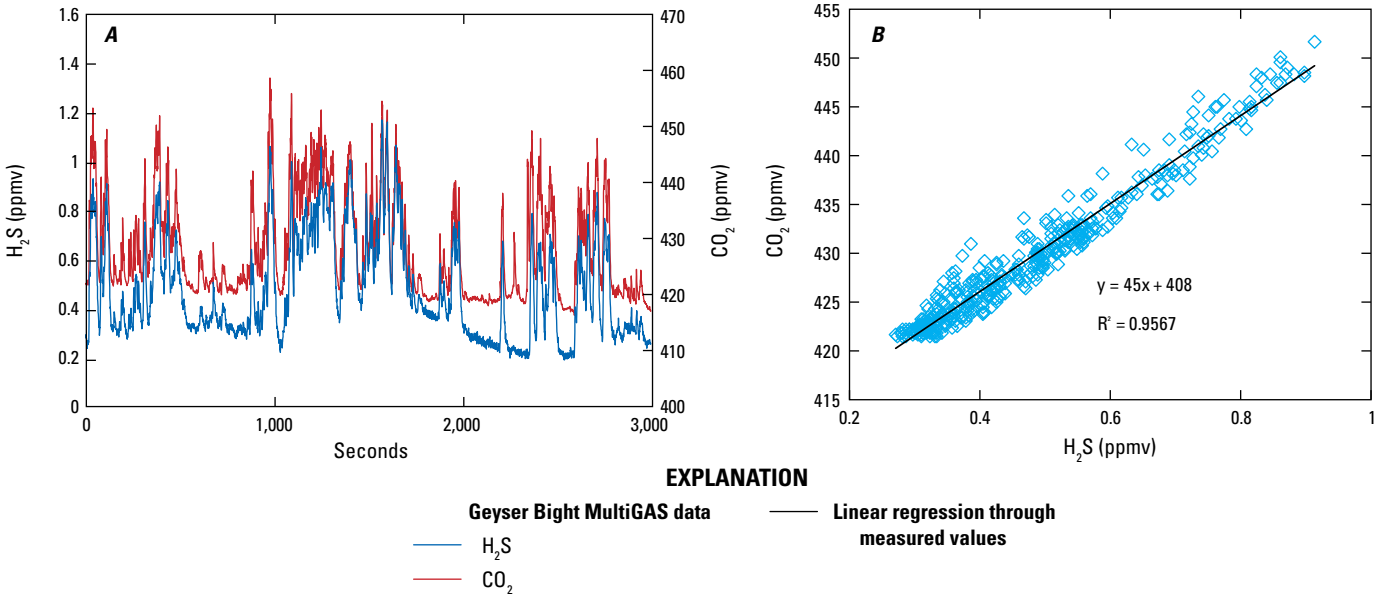

Figure 41. Graphs of MultiGAS data collected in the F1 area of Nye and others (1992) on Geyser Bight on August 16, 2015 (see figure 36 for location). *A*, Time series graph of the data with the peaks of CO_2 and H_2S corresponding in time (one sample per second). *B*, Graph displaying the regression of CO_2 to H_2S. Good correlation is observed between CO_2 and H_2S. CO_2/H_2S based on these data is about 45. Values are given in parts per million by volume (ppmv).

much lower gas concentrations and the correlation of CO_2 to H_2S was not as striking. Here, a CO_2/H_2S of 30 was calculated (fig. 42), which is similarly hydrothermal in nature.

Carbon and Helium Isotopes

The $\delta^{13}C$–CO_2 values for two samples of the upper and lower area gas were –13.0 and –15.8 per mil, respectively. The carbon isotope composition of the 2016 sample was –12.4 per mil, similar to the upper area gas in 2015 (Deb Bergfeld, personal communication, May 2017). The 2015 He sample from Geyser Bight was not analyzed due to the air contamination, and gas geothermometry could also not be utilized for the air-contaminated sample. To our knowledge the last He isotopic sample was collected in 1981 and gave a value of 7.4 (Nye and others, 1992).

Future Study Recommendations

Geyser Bight has long been recognized as an active hydrothermal area and hosts one of the hottest and largest hydrothermal systems in the Aleutian Islands. From a volcanological perspective, the heat source that supports the Geyser Bight hydrothermal system does not seem to have waned since the 1980s, as indicated by the constant temperatures. Geyser Bight also hosts one of the highest He isotopic signatures in the Aleutian Islands (7.4, Nye and others, 1992). Further geochemical measurements are warranted to fill in the gaps of this study in terms of sampling the areas not visited, obtaining gas samples that are not air contaminated, and attempting to remeasure the total heat output from the system. Because there were no apparent changes in the geochemical data from previous sampling, we suggest that the combined datasets provide a good assessment of the natural background conditions at Geyser Bight. Should there be geophysical evidence of renewed activity in the area of Mount Recheshnoi, new samples could be collected to look for evidence of higher heat output or greater volatile release.

Conclusions

Five volcano-hydrothermal areas in the Central Aleutians were visited in 2015 as part of an arc-wide National Science Foundation-funded initiative to study the Aleutian arc. The data represent valuable background information for these systems in terms of future volcanic hazard forecasting. Some of the areas had not been sampled in 20–30 years and some never sampled. Below is an executive summary of the findings.

At Makushin Volcano, the thermal expression seemed much less extensive than reported in the 1980s (Motyka and others, 1983, 1988), but this observation could have been influenced by poor weather conditions and limited accessibility. The compositions of the 2015 water samples were similar in character to that previously reported, but much more dilute. Dramatic reductions in SO_4 (and HCO_3) suggest less input from a shallow magmatic source, which is likely the result of reduced upflow of gas and heat in 2015 compared to the 1980s. This hypothesis is supported by the increase in the CO_2/H_2S ratio measured in gas emitting in 2015 (50) relative to that emitting in 1982 (8) or 1996 (15). Overall the findings are consistent with the reduction in the influence of shallow magmatism on the geochemistry of waters

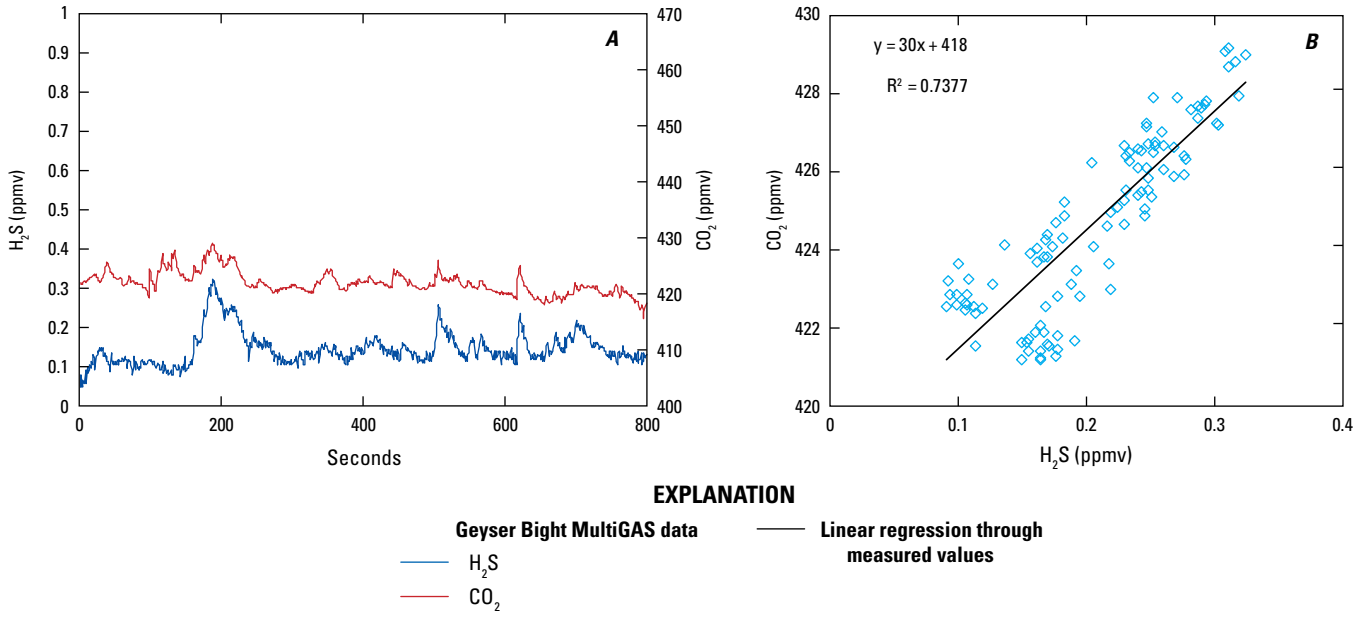

Figure 42. Graphs of MultiGAS data from the "G" hydrothermal area of Nye and others (1992) on Geyser Bight on August 16, 2015 (see figure 36 for location). Much lower gas concentrations were observed. (*A*) Time series graph of the data with the peaks of CO_2 and H_2S corresponding in time (one sample per second). (*B*) Graph displaying the regression of CO_2 to H_2S. Good correlation is observed between CO_2 and H_2S. CO_2/H_2S based on these data is about 30. Values are given in parts per million by volume (ppmv).

or a reduction in upflow from the hydrothermal reservoir. Future studies should attempt to characterize the summit region because it was not accessible in 2015. More comprehensive sampling in the UGV near Makushin volcano would also be warranted.

At Akutan Volcano, sampling was conducted in the flank fumarole area and along Hot Springs creek. A brief overflight of the summit did not detect volcanic gas in the caldera region, which is consistent with visual observations of weak degassing on the summit cone. Overall, the spring and gas results are very similar to that published by Bergfeld and others (2014) and Stelling and others (2015). Spring chemistry along Hot Spring creek was nearly identical to that previously published, and the composition of waters sampled in the flank fumarole area documented that no deep geothermal water was being released at that time. Gases were also nearly identical in composition to those sampled previously and are consistent with a mixed magmatic-hydrothermal origin. The CO_2/H_2S ratio as measured by the MultiGAS instrument (57) was similar to that measured in the fumaroles (up to 48) and was consistent with gas compositions typical of hydrothermal areas where sulfur species are removed from the gas stream due to scrubbing. Future volcano hazard studies should focus on the summit and flank fumarole area, sampling particularly for He isotopes and looking for changes in volcanic degassing (particularly the emergence of SO_2 and lower C/S) in the summit region).

Hydrothermal activity had not been recognized on Tana volcano until 2014, and the first water samples were collected that year (Evans and others, 2015). Sampling in 2015 was conducted high on the north flank and along the east coast near sea level and included both water and gas samples. The 2015 results complement those from 2014 (Evans and others 2015) and allow for better understanding of the different areas. All features are hydrothermal in character and those along the east coast are influenced by seawater. The data do not suggest there is outflow from a hydrothermal reservoir such as that observed at Akutan Volcano or Geyser Bight, rather they indicate that upflowing magmatic gases react with groundwaters to produce steam-heated regions where there is outflow of gas, but little fluid. The $\delta^{13}C$ and He isotope (R_c/R_a) compositions of the gases collected along the eastern coast were –9.7 and 6.43, respectively, representative of a magmatic signature. The CO_2/H_2S ratios as measured by the MultiGAS instrument were lower on the north flank (23) than along the coast (93), which may represent more scrubbing of soluble volatile components in the east. No gas samples were obtained from the north flank, and future excursions to the area should focus on this area as it shows the more magmatic chemical signatures.

Whereas thermal activity in Fisher Caldera had been noted in previous geological studies, the 2015 samples of gases and waters were the first of their kind for this area. Fumarolic samples were collected at mount Finch, the site of the last eruption, and spring and lake samples were collected in the caldera. The water from Turquoise lake was highly acidic (Turquoise cone is a previous volcanic vent), and interesting mixing relationships were observed between the caldera lakes, springs, and stream samples. The $^3He/^4He$ isotopic ratio (8.08) from fumarole gas is consistent with the highest measurements reported in Alaska after that from Mount Griggs (8.12) (Symonds and others, 2002). The helium and carbon isotope ratios (–7.3) are characteristic of upper mantle volatiles and the helium isotopes show that these gases have the least amount of crustal contamination of all gases collected in 2015 in the central Aleutian Islands. The CO_2/H_2S ratio as measured at mount Finch by the MultiGAS instrument (18–21) was lower than in the other hydrothermal areas, perhaps indicating stronger upwelling of gas or less scrubbing by hydrothermal waters. Future sampling in the area with relation to volcanic hazard should focus on mount Finch and Turquoise lake.

Finally, Geyser Bight has supported a persistent hydrothermal area, detailed studies of which took place in the 1980s (Nye and others, 1992; Motyka and others, 1993). Three of the six main hydrothermal areas were visited in 2015, though extensive sampling could not be completed due to the expanse of the area and limited time. Overall the chemistry data are very similar to that previously published, and, when combined with geothermometry results, demonstrate a robust heat source and overall stability of the system. Springs in the upper fumarole region had little Cl relative to SO_4, which is consistent with the lack of hydrothermal parent water issuing in this area. Here CO_2/H_2S as measured by the MultiGAS instrument (45) was higher than that measured down in the valley (30) where the majority of water outflow occurred, and gas concentrations were very low in the valley. Waters had high concentrations of arsenic (As) and barium (Ba), as previously noted (Motyka and others, 1993). Gas samples were contaminated by air, and thus not suitable for He isotopic measurement. From a volcanological perspective, the Geyser Bight area seems fairly stable given the similarity in data between the 1980s and 2015. Future studies should repeat the measurements for total heat output, which was measured in the 1980s, and attempt to locate the superheated fumarole 4 km southwest of the main thermal valley which was not visited in this study.

References Cited

Allard, P., 1983, The origin of hydrogen, carbon, sulfur, nitrogen and rare gases in volcanic exhalations: evidence from isotope geochemistry, in Tazieff, H., and Sabroux, J.-C., eds., Forecasting Volcanic Events: Amsterdam, Elsevier, p. 337–386.

Bergfeld, D., Lewicki, J.L., Evans, W.C., Hunt, A.G., Revesz, K., and Huebner, M., 2014, Geochemical investigation of the hydrothermal system on Akutan Island, Alaska, July 2012: U.S. Geological Survey Scientific Investigations Report 2013–5231, 20 p., https://pubs.usgs.gov/sir/2013/5231/.

Chiodini, G., Caliro, S., Lowenstern, J.B., Evans, W. C., Bergfeld, D., Tassi, F., Tedesco, D., 2012, Insights from fumarole gas geochemistry on the origin of hydrothermal fluids on the Yellowstone Plateau, Geochimica et Cosmochimica Acta, v. 89, p. 265–278, https://doi.org/10.1016/j.gca.2012.04.051.

D'Amore, F. and Panichi, C., 1980, Evaluation of deep temperatures of hydrothermal systems by a new gas geothermometer; Geochimica et Cosmochimica Acta, v. 44, p. 549–556.

Evans, W.C., Bergfeld, D., Neal, C.A., McGimsey, R.G., Werner, C.A., Waythomas, C.F., Lewicki, J.L., Lopez, T., Mangan, M.T., Miller, T.P., Diefenbach, A., Schaefer, J., Coombs, M.L., Wang, B., Nicolaysen, K., Izbekov, P., Maharrey, Z., Huebner, M., Hunt, A.G., Fitzpatrick, J., and Freeburg, G., 2015, Aleutian Arc geothermal fluids; chemical analyses of waters and gases sampled in association with the Alaska Volcano Observatory: U.S. Geological Survey Data Release, https://doi.org/10.5066/F74X55VB.

Ewert, J.W., Diefenbach, A.K., and Ramsey, D.W., 2018, 2018 update to the U.S. Geological Survey national volcanic threat assessment: U.S. Geological Survey Scientific Investigations Report 2018–5140, 40 p., https://doi.org/10.3133/sir20185140.

Ewert, J.W., Guffanti, M., and Murray, T.L., 2005, An assessment of volcanic threat and monitoring capabilities in the United States; framework for a National Volcano Early Warning System: U.S. Geological Survey Open-File Report 2005–1164, 62 p., https://doi.org/10.3133/ofr20051164

Giggenbach, W.F., 1980. Geothermal gas equilibria: Geochimica et Cosmochimca Acta, v. 44, p. 2021–2023.

Giggenbach, W.F., 1988, Geothermal solute equilibria. Derivation of Na-K-Mg-Ca geoindicators. Geochimica et Cosmochimca Acta, v. 52, p. 2749–2765.

Giggenbach, W.F. and Goguel, R.L., 1989. Collection and analysis of geothermal and volcanic water and gas discharges: Petone, New Zealand, Department of Scientific and Industrial Research—Chemistry Division, 81 p.

Gong, W., Meyer, F. J., Lee, C. W., Lu, Z., and Freymueller, J., 2015, Measurement and interpretation of subtle deformation signals at Unimak Island from 2003 to 2010 using weather model-assisted time series InSAR: Journal of Geophysical Research; Solid Earth, v. 120, no. 2, p. 1175–1194.

Lu, Z., Dzurisin, D., 2014, InSAR Imaging of Aleutian Volcanoes—Monitoring a Volcanic Arc From Space: Heidelberg, New York, Springer Praxis Books, Geophysical Sciences, 388 pp.

Mann, Dorte, and Freymueller, J., 2003, Volcanic and tectonic deformation on Unimak Island in the Aleutian Arc, Alaska: Journal of Geophysical Research, v. 108, no. 2, p. 1–12.

Motyka, R.J., Liss, S.A., Nye, C.J., and Moorman, M.A., 1993, Geothermal resources of the Aleutian Arc: Alaska Division of Geological and Geophysical Surveys Professional Report 0114, 17 p., 4 sheets, scale 1:1,000,000.

Motyka, R.J., Moorman, M.A., and Poreda, Robert, 1983, Progress report—thermal fluid investigations of the Makushin geothermal area: Alaska Division of Geological and Geophysical Surveys Report of Investigations 83-15, 52 p., https://doi.org/10.14509/2354.

Motyka, R.I., Queen, L.D., Janik, C.J., Sheppard, D.S., Poreda, R.J., and Liss, S.A., 1988, Fluid geochemistry and fluid mineral equilibria in test wells and thermal gradient holes at the Makushin geothermal area, Unalaska Island, Alaska: Alaska Division of Geological and Geophysical Surveys, Report of Investigations 88-14, 90 p., https://doi.org/10.14509/2462

Neal, C.A., McGimsey, R.G., Dixon, J.P., Cameron, C.E., Nuzhdaev, A.A., and Chibisova, Marina, 2011, 2008 Volcanic activity in Alaska, Kamchatka, and the Kurile Islands—Summary of events and response of the Alaska Volcano Observatory: U.S. Geological Survey Scientific Investigations Report 2010–5243, 94 p., https://pubs.usgs.gov/sir/2010/5243/.

Nye, C. J., Motyka, R. J., Turner. D. L. and Liss, S. A., 1992. Geology and geochemistry of the Geyser Bight Geothermal Area, Umnak Island. Aleutian Islands, Alaska. Alaska Division of Geological and Geophysical Surveys, Report of Investigation 92-I, 85 pp., 2 sheets, scale 1:24,000. https://doi.org/10.14509/2480

Powell, T., and Cumming, W, 2010, Spreadsheets for geothermal water and gas geochemistry. Proceedings of the Thirty-Fifth Workshop on Geothermal Reservoir Engineering, Stanford University, Stanford, California, February 1–3, 2010, SGP-TR-188.

Stelling, P.L., Gardner, J.E., and Begét, J.E., 2005, Eruptive history of Fisher Caldera, Alaska, USA: Journal of Volcanology and Geothermal Research, v. 139, no. 3–4, p. 163–183.

Stelling P., Hinz, N.H., Kolker, A., Ohren, M., 2015, Exploration of the Hot Springs Bay Valley (HSBV) geothermal resource area, Akutan, Alaska: Geothermics, v. 9, no. 57, p.127–144.

Symonds, Robert B, Janik, C J, Evans, W C, Ritchie, B E, Counce, Dale, Poreda, R J, and Iven, Mark, 2003, Scrubbing masks magmatic degassing during repose at Cascade-Range and Aleutian-Arc volcanoes: United States Geological Survey Open File Report 03–435, 22 p., https://pubs.usgs.gov/of/2003/0435/.

Symonds, Robert B, Poreda, Robert J, Evans, William C, Janik, Cathy J, and Ritchie, Beatrice E, 2003, Mantle and Crustal Sources of Carbon, Nitrogen, and Noble gases in Cascade-Range and Aleutian-Arc Volcanic gases: United States Geological Survey Open File Report 03–436, 26 p., https://pubs.usgs.gov/of/2003/0436/.

Werner, C, Evans, W C, Poland, M, Tucker, D S, and Doukas, M P, 2009, Long-term changes in quiescent degassing at Mount Baker Volcano, Washington, USA; Evidence for a stalled intrusion in 1975 and connection to a deep magma source: Journal of Volcanology and Geothermal Research, v. 186, no. 3–4, p. 379–386.

Werner, C., Kern, C., Coppola, D., Lyons, J. J., Kelly, P. J., Wallace, K. L., Schneider, D. J., Wessels, R. L., 2017, Magmatic degassing, lava dome extrusion, and explosions from Mount Cleveland volcano, Alaska, 2011–2015—Insight into the continuous nature of volcanic activity over multi-year timescales, Journal of Volcanology and Geothermal Research, v. 337, p. 98–110, https://doi.org/10.1016/j.jvolgeores.2017.03.001.

Menlo Park Publishing Service Center, California
Manuscript approved for publication March 16, 2020
Edited by Phil A. Frederick
Cartography and illustration support by JoJo Mangano
Layout and design by Cory D. Hurd

USGS

Werner and others—**Chemical Evaluation of Water and Gases Collected from Hydrothermal Systems**—Scientific Investigations Report 2020–5043, August 2015

ISSN 2328-0328 (online)
https://doi.org/10.3133/sir20205043